POLITECNICO DI TORINO

Corso di Laurea
in Ingegneria Elettronica

Tesi di Laurea

Graphene-based sensor of aflatoxin molecule: a simulation-based investigation

Relatori
Prof. Gianluca Piccinini
Prof. Mariagrazia Graziano
M.Eng. Fabrizio Mo
M.Eng. Chiara Elfi Spano

Candidato
Walter Ala

Anno Accademico 2022-2023

Summary

For some years now the unique electronic properties of graphene have attracted interest in this material. There are many research areas that involve it, from high-speed electronics to sensors. The latter together with molecular electronics promise the creation of graphene sensors capable of identifying individual molecules. This is the sector in which this thesis work belongs, in which graphene is analyzed as a possible sensor for the aflatoxin molecule.

In the first part the main characteristics of graphene are reviewed, with its physical structure, the particular electronic band structure, the transport behavior, the density of the states, its finite-dimensional structures, the presence of defects and the doping. The aflatoxin molecule is described with its peculiarities and the reasons for its danger. Finally, the characteristics of the adsorption process and the use of graphene as a sensor are indicated, selecting some related research and works.

In the second part, graphene is investigated as a possible sensor for the aflatoxin molecule. Through simulations of the Quantum ATK software package, the adsorption of the molecule on graphene is first analyzed by investigating the adsorption energy for various geometric configurations and then graphene is examined as a sensor by analyzing its sensitivity and selectivity.

The result obtained is that graphene has a good sensitivity with respect to aflatoxin, identifiable through a variation of the current in the presence and absence of the molecule, but it is not very selective, as a very similar behavior is observed with some other molecules.

Acknowledgements

I would like to thank M.Eng. F. Mo and M.Eng. C.E. Spano for their suggestions and indications during the thesis work.

I would like to thank Prof. G. Piccinini and Prof. M. Graziano for having me in their working group.

I would like to thank my family and loved ones for the support they have gave me.

Contents

List of Tables

List of Figures

Part I

Part one

Chapter 1

Introduction

Aflatoxins are a set of mycotoxins which are produced by some fungi of the *Aspergillus flavus* and *Aspergillus parasiticus* type which contaminate some types of agricultural products and are more common in hot and humid areas of the world. They are toxic, carcinogenic, mutagenic and immunosuppressive. Aflatoxin B1 turns out to be the most dangerous. The danger to human and animal health derives mainly from the ingestion of contaminated food. From this danger derives the importance of being able to identify their presence. Today, the detection of aflatoxins is still an open field, in which we observe the development of techniques and methods in the research and laboratory phases with the promise that in the near future they will be able to overcome the difficulties of today's methods. Indeed, the latter normally used for detection of aflatoxin require the use of a laboratory, expensive instrumentation, complex processes, specialized personnel and long response times. For example, extraction, clean up and subsequent separation techniques are used for the identification and measurement of the molecule, with high costs. There is a need for fast-response, easy-to-use and cost-effective detection methods to readily ensure food safety at various stages, from production to storage and distribution. Nanomaterials appear to be a promising answer. Nanomaterial sensor seem capable of detecting the molecule in a simpler way, with high sensitivity and high selectivity.[1] [2]

Numerous biosensors have been studied with this aim. Today nanomaterials combined with biosensors are used to improve sensitivity, preparation time and molecule detection. [1] Metal nanomaterials can be combined with different type biological macromolecules such as antibodies, aptamers, enzymes by improving the adsorption characteristics. [3] Metal oxide and hydroxides nanomaterials allow to improve the performance of biosensors.[4] [5] Among the disadvantages we find the use of toxic nanomaterials and the high manufacturing costs.

The use of nanomaterials through molecular electronics allows for reusable sensors, operating on site and in real time with automatic measurement. Important advantages that push research in this direction. Developments in molecular electronics have allowed for improved research into single molecule detection. [6] [7] The use of materials such as graphene, carbon nanotube fullerenes are introduced. Carbon-based nanomaterials

exhibit excellent electrical and adsorption properties, biocompatibility, and the possibility of functionalization. An example is an ultrasensitive electrochemiluminescence (ECL) sensor for aflatoxin M1. [2].

The study of a sensor for aflatoxin B1 with the use of graphene fits into this scenario of molecular electronics.

In frame of this thesis, I investigate graphene as a possible sensor for the aflatoxin B1 molecule through the use of DFT simulations with software QuantumWise ToolKit (ATK). In order to reach this result, I aim to analyze the adsorption phase of the molecule on graphene in various geometric positions. Then I plan to verify the sensitivity of the sensor to the molecule in various configurations and finally to investigate the selectivity of the sensor with respect to other molecules present in the environment.

1.1 Organization of this work

My thesis work is divided into two parts. In the first part I summarize important theoretical concepts on graphene, aflatoxin, adsorption and graphene sensor. In the second part I submit the analyzes and the results of the simulations. In the following I present a brief description of the topics of the various chapters.

Part I

- In chapter 1 we have seen a description of the general scenario in which this thesis work is located, the motivations and the importance in the realization of a sensor for aflatoxin B1.
- In chapter 2 I will present the main characteristics of graphene and its physical structure. I will describe its electronic properties, band structure and how it is obtained. I will talk about the characteristics of its transport phenomena, current, conductance and low bias behavior; its density of states and electron carrier density. Then a word on nanoribbon formation. Finally I will describe the presence of defects in the graphene layer and the presence of doping.
- In chapter 3 I will present the main characteristics of aflatoxin, I will explain what it is, how it is produced and how it spreads; its presence in agricultural products and animal feed; its danger to human health and therefore the need to detect and manage it.
- In chapter 4 I will talk about the adsorption process, a phenomenon that involves the surface of materials. It is divided into physisorption and chemisorption based on the type of interactions that are created. Then I will present the characteristics of this process on graphene presenting some research in addition.
- In chapter 5 I will focus on graphene used as a sensor. I will describe its properties and some research works based on it.

Part II

- In chapter 6 I will describe the methodological steps followed and the computational methods used for the simulations and I will show the tables with their parameters.
- In chapter 7 I will analyze the simulations related to the adsorption of AFB1 on the graphene: eight different configurations of the molecule on the graphene layer, their adsorption energies, to find the most stable configuration. Then I will investigate the variation of the adsorption energy with respect to the adsorption site on the graphene.
- In chapter 8 I will present the simulations using a device made with graphene channel and with electrodes in graphene also. I will investigate the sensitivity of the sensor through the variation of the current in the presence and absence of AFB1. I will do this with AFB1 in the two most stable adsorption configurations. Then I will analyze the sensitivity by replacing the graphene in the channel with a passivated nanoribbon. Finally I will analyze the sensitivity of the sensor with respect to other molecules that may be encountered in the workplace of device.
- In chapter 9 I will summarize the work done and I will draw conclusions. Also I will present some ideas for solving the problems encountered and possible future research.

Chapter 2

Graphene

2.1 Physical structure, properties

Graphene has attracted the attention of researchers and the scientific community for its exceptional thermal, mechanical and electronic properties. As far as the electronic field great hopes are placed in its possible use in devices and applications concerning nanoelectronics.

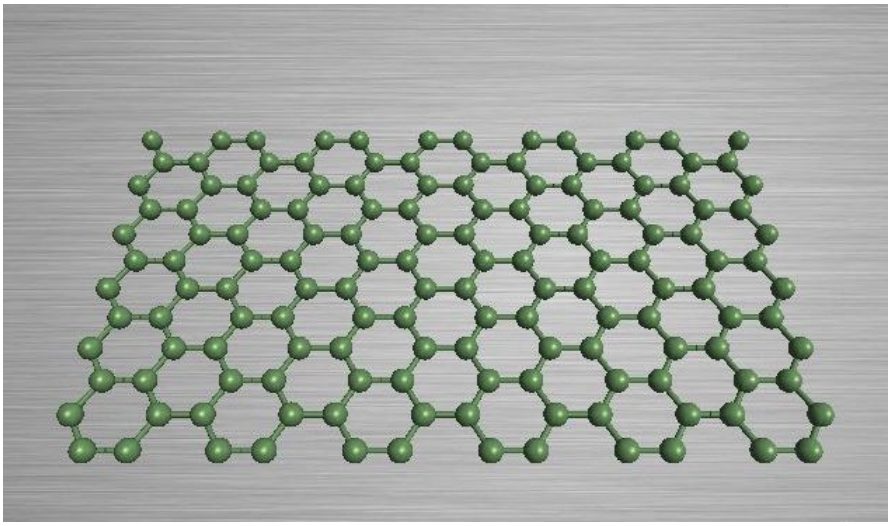

Figure 2.1: Graphene layer.

Graphene is a material composed of a single layer of carbon atoms bonded together by strong covalent bonds and forming a hexagonal honeycomb lattice. Carbon atoms have an electronic structure of $2s^2\ 2p_x\ 2p_y$. The distribution of a single electron around the nucleus is described through a wave function called orbital. When these elementary orbitals interact with those of other atoms, molecular orbitals are formed. In the case of carbon, the four valence electrons of the carbon atom tend to bond with those of other

carbon atoms to form crystals. The interaction between the atomic orbitals of an atom with those of the closest atoms creates the formation of new molecular orbitals called hybrids. The different types of hybridization leads to the formation of different carbon allotropes (fullerene, carbon nanotubes...)[8].

In graphene the carbon atoms form covalent bonds arranged in a single plane. One s orbital and two p orbitals interact to form $3sp^2$ hybrid orbitals. These orbitals give rise to three bonds called σ which are stronger than traditional covalent bonds and are positioned parallel to the plane of union of the nuclei of carbon atoms. The electron distribution of such bonds is localized along the plane of the atoms. The only remaining electron of the four starting valence electrons, goes to occupy the orbital $2p_z$, which turns out to be perpendicular to the plane that joins the atoms together. These orbitals form bonds called π. Thanks to the particular structure, graphene presents extraordinary properties. The formation of sigma bonds, the result of hybridization, parallel to the graphene plane, give strength and flexibility to the material resulting in a high breaking strength and a high Young's modulus. The electrons of the σ bonds are localized. As far as the electronic properties are concerned, they are due to the π and π^* (antibonding) orbitals obtained from the hybridization of the p_z bonds which are perpendicular to the plane of the graphene and give rise to an electronic gas capable of moving along the graphene plane, resulting in a large electrical conductivity.[8] [9]

2.2 Band structure

The construction of the graphene band structure is the starting point for understanding the extraordinary properties of this material. The carbon atoms in graphene are arranged in a hexagonal lattice. But not all carbon atoms are equal to each other, in fact if one takes two atoms bonded to each other one can easily see that what each of them sees on the left and right is different. Consequently, a single carbon atom cannot be used as a unit cell of the lattice. However, if we consider the structure of graphene as composed of two triangular sublattices (A and B) interpenetrated to form the hexagonal honeycomb lattice, we realize that each A atom is linked only to B atoms and vice versa. We can then take as a unit cell the one formed by two atoms, one belonging to A and one belonging to B and adjacent to each other (Figure 2.2). There are therefore two π electrons per unit cell (one for each atom) which contribute to the electronic properties of graphene [10].

The mathematical construction of the reciprocal lattice allows us to study the properties of graphene with greater understanding. We perform a transformation from the real lattice to the reciprocal lattice, also called k-space. Every point in the Brillouin zone in the reciprocal lattice can be reached through the wave vector k. The reachable points within this zone correspond to the states allowed in the dispersion relation. So, the Brillouin zone contains all the energy solutions allowed by the crystalline solid.

The relationship between real lattice space and reciprocal lattice space is the same as between time and frequency, which can be expressed by the sum of the Fourier components. To pass from the real space to the reciprocal space we express the primitive vectors of the reciprocal lattice as a function of the primitive vectors of the real lattice. [8]

In the figure (2.3) representing the real or direct lattice, the primitive vectors $\mathbf{a_1}$ and

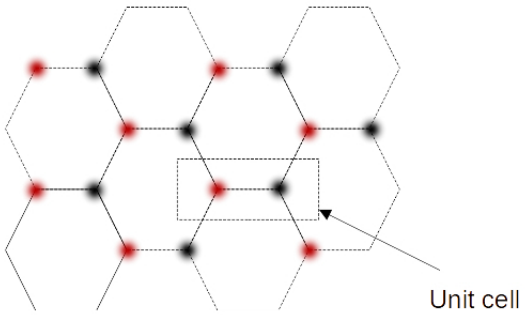

Figure 2.2: The honeycomb lattice of graphene. Unit cell composed of one atom of A (red) and one atom of B (black)

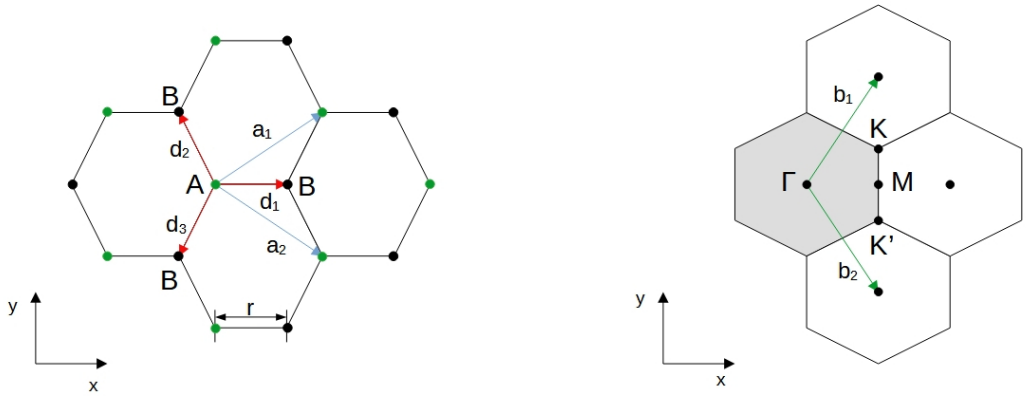

(a) Direct lattice

(b) Reciprocal lattice

Figure 2.3: Graphical representation of the two lattices, direct and reciprocal

$\mathbf{a_2}$ are displayed:

$$\mathbf{a_1} = \frac{1}{2}(\sqrt{3}a_0, a_0) \qquad \mathbf{a_2} = \frac{1}{2}(\sqrt{3}a_0, -a_0)$$

with $a_0 = \sqrt{3}r$ where r is the length of the side of the hexagon (r = 1,42 Å) and $|\mathbf{a_1}| = |\mathbf{a_2}| = a_0$. Each atom of sublattice A is bonded to three atoms of sublattice B through vectors $\mathbf{d_1}$, $\mathbf{d_2}$, $\mathbf{d_3}$ with $|\mathbf{d_1}| = |\mathbf{d_2}| = |\mathbf{d_3}| = r$. From the figure (2.3a) we can get:

$$\mathbf{d_1} = (r,0) = \left(\frac{a_0}{\sqrt{3}}, 0\right)$$

$$\mathbf{d_2} = -\mathbf{a_2} + \mathbf{d_1} = \frac{1}{2}\left(-\frac{a_0}{\sqrt{3}}, -a_0\right)$$

$$\mathbf{d_3} = -\mathbf{a_1} + \mathbf{d_1} = \frac{1}{2}\left(-\frac{a_0}{\sqrt{3}}, a_0\right)$$

The reciprocal lattice is also a hexagonal honeycomb lattice but rotated 90º degrees from the real lattice. Its primitive vectors are $\mathbf{b_1}$ and $\mathbf{b_2}$

$$\mathbf{b_1} = \frac{2\pi}{a_0}\left(\frac{1}{\sqrt{3}}, 1\right) \qquad \mathbf{b_2} = \frac{2\pi}{a_0}\left(\frac{1}{\sqrt{3}}, -1\right)$$

There are three points of high symmetry resulting from the reciprocal lattice. Γ-point is the central point of the Brillouin zone, K-point (including K and K') are the corners of the Brillouin zone and M-point midpoints of the sides of the Brillouin zone. The K-points are those of greatest interest, they are the points where the conduction and valence bands touch. [11]

Starting from first principles it is possible to calculate numerically the band structure of graphene shown in figure 2.4. The various energy branches are due to the outermost electrons of the σ and π bonds of the carbon atoms.

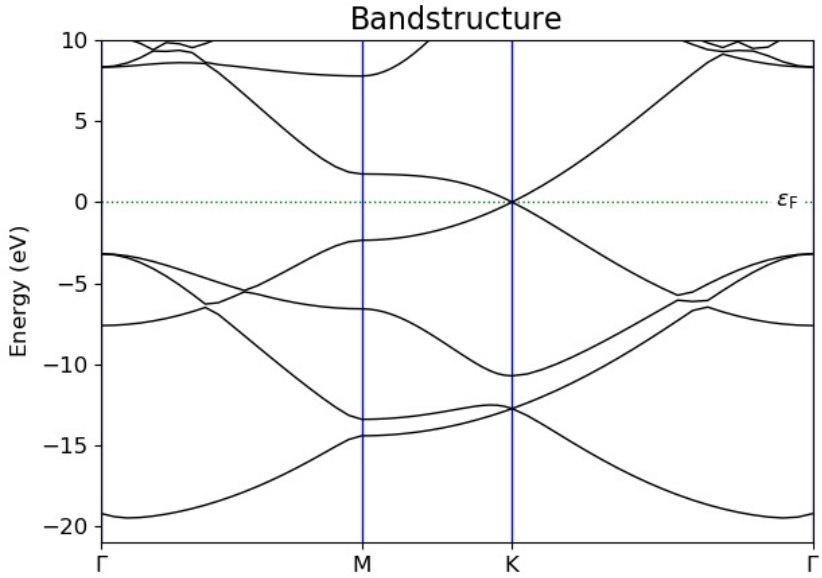

Figure 2.4: Band structure 2D of graphene pure

We can also look for an analytical solution for the electronic band structure of graphene by exploiting models that make some approximations. The starting point is the Schrödinger equation. The resolution of its time-independent equation. This equation is a description of the system under study:

$$H\Psi(k, r) = E(k)\Psi(k, r) \tag{2.1}$$

where H is the Hamiltonian operator, representing the total energy of the system and is composed of the sum of the terms of kinetic energy and potential energy. For an electron in a periodic solid it can be written as:

$$H = \frac{\hbar^2}{2m}\nabla^2 + \sum_i^N U(\mathbf{r} - \mathbf{R_i}) \tag{2.2}$$

In the equation of Schrödinger, H acts on the wave function Ψ of the electron and allows to obtain the energy values allowed to the electron in the system. Substituting (2.2) into (2.1), we get a second order partial differential equation. We need to find a wave function solution of this equation that satisfies Bloch's theorem in a crystalline solid. To satisfy the Bloch conditions the wave function must satisfy the equation of waves traveling in a lattice:

$$\Psi(\mathbf{r} + \mathbf{R}) = e^{i\mathbf{k}\cdot\mathbf{R}}\Psi(\mathbf{r}) \tag{2.3}$$

and the boundary conditions:

$$\Psi(\mathbf{r}) = \Psi(\mathbf{r} + \mathbf{S}) = e^{i\mathbf{k}\cdot\mathbf{S}}\Psi(\mathbf{r}) \tag{2.4}$$

therefore: $e^{i\mathbf{k}\cdot\mathbf{S}} = 1$

To solve this problem, the most used technique exploits the tight binding model. This model exploits the linear combination of atomic orbitals. More precisely the $2p_z$ atomic orbitals. This model:

- assumes that the outermost electrons of atoms are mainly located at their respective atomic nuclei, can consequently be described by their atomic orbitals, and are therefore characterized by their discrete energy levels
- in the solid, however, the atoms are not isolated, so the atomic orbitals of the electrons of the closest atoms overlap, consequently the discrete energy levels broaden to the creation of almost continuous energy bands, composed of a certain number of states which satisfy the Pauli exclusion principle. So only the interactions between nearest neighbors are considered.

The use of atomic orbitals in the description of electrons is an approximation because there is an overlap of wave functions, so the results obtained must be confirmed by experimental tests or more precise *ab initio* calculations. However, this technique allows to obtain an analytical description of the band structure and is of great help for the study of electronic properties. Through analytical calculations with the use of the tight binding model, the formula for the description of the band structure of graphene is obtained [8]:

$$E(\mathbf{k}) = \pm t\sqrt{4\cos^2\left(\frac{a_0 k_y}{2}\right) + 4\cos\left(\frac{a_0 k_y}{2}\right)\cos\left(\frac{\sqrt{3}a_0 k_x}{2}\right) + 1} \tag{2.5}$$

where t is a parameter estimated as 3.15 eV and it features the nearest neighbor interactions. [12] In the figure (2.5) there is a graphical 3D representation.

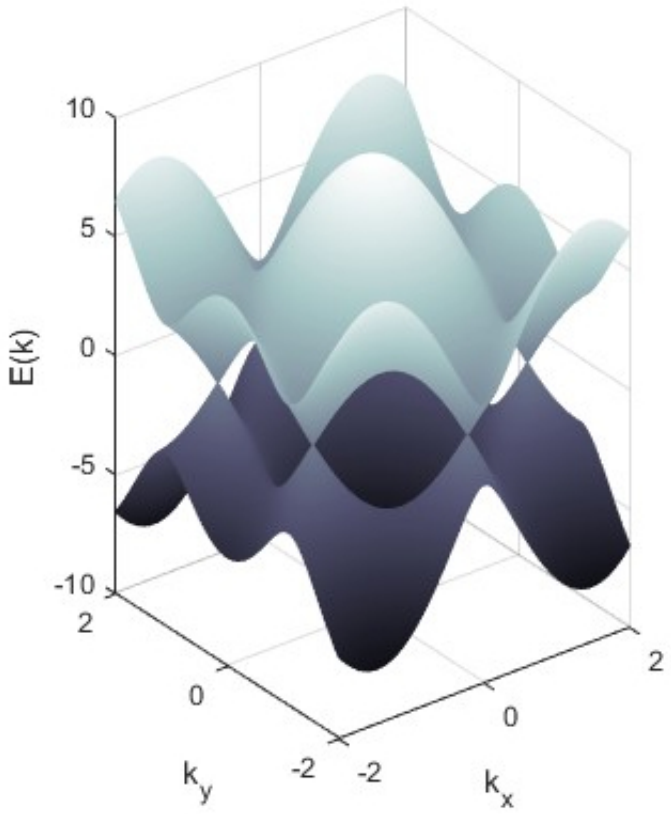

Figure 2.5: 3D electronic band structure of graphene pure obtained by tight-binding model.

As we have already anticipated when speaking of the reciprocal lattice, the conduction and valence bands degenerate in six points, where they come into contact, corresponding to the corners of the hexagon representing the Brillouin zone. These six points are divided into two groups, K and K', called valleys. Points K and K' are essentially equivalent for most purposes. These points are called Dirac points. [8]

2.2.1 Dirac equation

Near the Dirac point the charge carriers in graphene behave as if they were massless relativistic particles, so very often to derive the material properties the starting point is the Dirac equation which can be written in the form:

$$E \begin{Bmatrix} \Psi \\ \Theta \end{Bmatrix} = \begin{bmatrix} (mc^2 + U)I & c\vec{\sigma} \cdot \vec{p} \\ c\vec{\sigma} \cdot \vec{p} & (-mc^2 + U)I \end{bmatrix} \begin{Bmatrix} \Psi \\ \Theta \end{Bmatrix} \tag{2.6}$$

Starting from this equation (2.6) and using a non-relativistic approximation we obtain

$$E(\Psi_1) = [H_1](\Psi_1) \tag{2.7}$$

where Ψ_1 is composed from two component, up-spin and down-spin, of electronic wave function and H_1 is a matrix. From this equation the band structure of graphene can be obtained. [10]

2.3 Transport and current

To understand the phenomenon of transport in graphene we can start from the general model for calculating the current in a nanoscale device. This model tells us that the current can be described by the equation [13]:

$$I = \frac{2q}{h} \int T(E)M(E)(f_1 - f_2)\, dE \tag{2.8}$$

where:

- $T(E)$ is the Transmission Probability and it indicates the probability with which an electron at energy E injected from contact 1 of the device manages to reach contact 2.
- $M(E)$ is the number of modes, and it indicates the number of channels conducting at a given energy E
- f_1 is equilibrium Fermi function at the contact 1, the source.
- f_2 is equilibrium Fermi function at the contact 2, the drain.

In using this formula, we assume that current flows through independent energy conductive channels. The formula can be used for any applied bias voltage, but as this voltage increases, the energy channels may no longer be independent and therefore this model would lose its validity. Instead in a situation of near equilibrium transport, for low bias, and with the same temperature of the two contacts, the current formula can be simplified by approximating the difference between the Fermi functions of the two contacts with the Taylor series expansion

$$(f_1 - f_2) \approx -\frac{\partial f}{\partial E_F} \Delta E_F$$

where:

$$f = f(E, E_F) = \frac{1}{1 + e^{\frac{E - E_F}{k_B T}}} \quad \text{is the equilibrium Fermi function}$$

and with $\Delta E_F = -qV$ substituting into the equation (2.8) we get [13]:

$$I = \left[\frac{2q^2}{h} \int T(E)M(E) \left(-\frac{\partial f}{\partial E} \right) dE \right] V \tag{2.9}$$

where the term in brackets is the conductance:

$$G = \frac{I}{V} = \frac{2q^2}{h} \int T(E)M(E)\left(-\frac{\partial f}{\partial E}\right) dE \tag{2.10}$$

Transport: diffusive, ballistic, quasi-ballistic

As we said T(E) represents the probability of transmission along the conductive channel and is given by the formula:

$$T(E) = \frac{\lambda(E)}{\lambda(E) + L} \tag{2.11}$$

where L is the length of the transport channel, λ is mean free path of the charge carriers and T(E) being a probability must be a number between 0 and 1.

We have 3 different types of possible transport: diffusive, ballistic, quasi-ballistic. All can be studied through this current model by changing the transmission probability [13].

Diffusive: the length of the channel is much greater than mean free path

$$L \gg \lambda \Longrightarrow T(E) = \frac{\lambda}{L} \ll 1$$

the probability of transmission of an electron from contact 1 to contact 2 of the device is much less than 1 mainly due to scattering phenomena.

Ballistic: the conductive channel is very short compared with the mean free path

$$L \ll \lambda \Longrightarrow T(E) \to 1$$

an electron entering the channel passes through it without undergoing scattering phenomena

Quasi-ballistic: the channel length and mean free path are of comparable size

$$L \approx \lambda \Longrightarrow T(E) < 1$$

Modes of conduction

As we have said, M(E) represents the number of modes that contribute to transport within the channel. Its formula changes according to the geometry of the device, whether in 1, 2 or 3 dimensions. For graphene, a 2D material we have:

$$M(E) = \frac{2|E|W}{\pi\hbar v_F} \tag{2.12}$$

where W is the width of the conductive channel of the device under study. So, in graphene the number of modes is linear with respect to energy and with respect to the width of the transport channel. [13]

2.3.1 Transport at low bias

Of significant interest is the behavior of electrons in the vicinity of the energy where the conduction and valence bands meet. As it can be seen from the figure (2.5), the two bands touch each other in six vertices of the Brillouin zone. But only two of them are distinct, while the others can be reached through reciprocal lattice vectors. This energy level under charge-neutral conditions is the Fermi energy level. All electronic states below this level are full and all states above are empty. The points of contact are called Dirac points or points of neutrality (Fig. 2.6). Near these points, therefore at low energies, the linear trend of the dispersion relation can be seen

$$E = \pm\hbar v_f |\mathbf{k}| = \pm\hbar v_f \sqrt{k_x^2 + k_y^2} \tag{2.13}$$

where $\mathbf{k}$ is wavevector in two dimensions (x and y) of charge carriers relative to Dirac points, $\hbar$ is the reduced Planck's constant and v_f is the Fermi velocity:

$$v_f = \left(\frac{1}{\hbar}\right)\left(\frac{\partial E}{\partial k}\right) \tag{2.14}$$

At low bias transport we note that this speed is constant, independent of $\mathbf{k}$, has a value of about 1 x 10^8 cm/s and for this very high value it has aroused considerable interest in high-speed electronics.

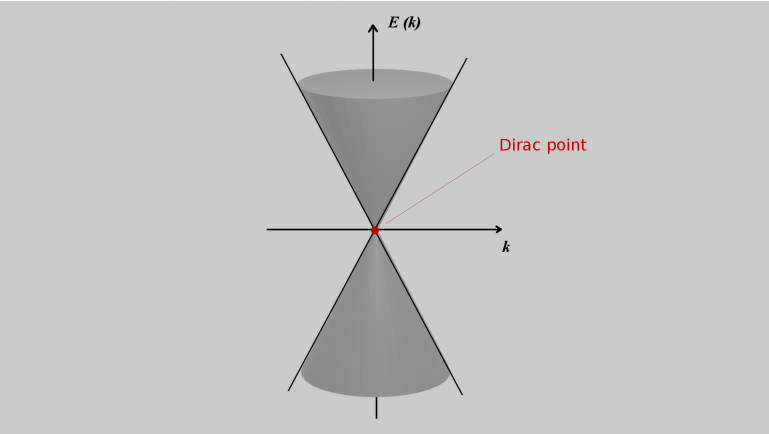

Figure 2.6: Representation of the band structure of graphene at low energies, near the Dirac point. The cone shape underlines the linear trend of the energy with respect to the wave vector.

Linear trend up to about ±0.6 eV. At higher energies, the deviation of the behavior compared to the linear trend is no longer negligible.

The linear trend is representative of massless particles, particles with zero effective mass. To describe such particles, the Dirac equation is used rather than the Schrödinger equation. [13] [8]

2.3.2 Density of states and electron carrier density

Now we calculate the density of states (DOS) and the density of charge carriers in the material. Graphene is a two-dimensional material. Given the dispersion relation, the total number of states available at a certain energy E is given by the number of states within the circle of radius k in the k-space, corresponding to the energy E. Its variation in correspondence with a variation dE of the energy is given by the ratio between the variation of the area dS in the k-space due to the variation dk and the area occupied by a single state. We can thus write:

$$\rho(E)dE = p\frac{dS}{\frac{(2\pi)^2}{A}} \tag{2.15}$$

where for graphene $p = 4$ for spin degeneracy and for valley degeneracy (K and K'), A is the area of the lattice.

The increase in area dS due to a very small change dk holds $2\pi k dk$, from which we get the density of states, number of states per unit of energy per unit area:

$$\rho(E) = \frac{2}{\pi}\left|k\frac{\partial k}{\partial E}\right| \tag{2.16}$$

Then substituting eq.(2.15) we get the equation of DOS for low energy for graphene [8]:

$$\rho(E) = \frac{2}{\pi\hbar^2 v_f^2}|E| \tag{2.17}$$

This means that the density of states (DOS) in graphene increases linearly with the absolute value of the energy, unlike conventional semiconductors in which the dispersion relationship is parabolic and therefore the density of states remains constant regardless of the energy. Although the density of states goes to zero at zero energy, there are no band gaps. Graphene is also different from metals; in fact, the latter have a high density of states at the Fermi energy.

The number of electrons is given by the number of states occupied per unit area at a given temperature. Given a temperature T, the probability of occupation of the states is obtained through the Fermi-Dirac distribution:

$$f(E,\mu) = \frac{1}{1 + e^{\frac{E-\mu}{k_B T}}}$$

The density of electrons at equilibrium:

$$n_e = \int_0^\infty \rho(E) f(E, E_f)\, dE \tag{2.18}$$

In the case of graphene substituting the eq.(2.17) found earlier for the density of states we get:

$$n_e = \frac{2}{\pi\hbar^2 v_f^2}\int_0^\infty \frac{E}{1 + e^{\frac{E-E_f}{k_B T}}}\, dE \tag{2.19}$$

For pure graphene the intrinsic carrier density is:

$$n_e = \frac{\pi k_B^2 T^2}{6\hbar^2 v_f^2} \approx 9 * 10^5 T^2 \quad [electrons/cm^2] \tag{2.20}$$

For symmetry in the band structure, we have the same value for the holes. It can be noted the dependence on the square of the temperature, different from that which occurs with traditional semiconductors. [8]

2.3.3 Graphene nanoribbons

From a graphene layer of infinite size, we pass to graphene layers of finite size which are called nanoribbons. Based on the type of edge obtained from the cut, they are divided into armchair or zigzag. The dangling bonds of the edge carbon atoms are passivated. They are structures with a width of less than 100 nm, in which the transport properties are influenced by the thickness of the structure itself.

The band structure is obtained by solving the Hamiltonian considering the confinement due to the presence of the edges. Depending on the number of atoms in the width, the behavior of the nanoribbon can be metallic, or have a band gap. [11]

2.4 Defects

We studied graphene as a pure material, with no defects in its physical structure. However, in the construction of a layer of graphene due to the manufacturing process, growth or separation, defects can be created inside it. These defects can degrade the performance of the material, or they can create new chemical and physical properties that can be exploited by new devices. We know that graphene has exceptional electronic properties. These properties arise from the electronic structure around the Fermi energy. The number and placement of electronic states near this energy level are responsible for the material's properties. The defects, as well as the edges in the nanoribbons, can give rise to new localized electronic states in the vicinity of the Fermi energy, thus capable of changing the properties of the material. These new states increase the density of the states around the Fermi energy and therefore there is an increase in electrons at these energy levels. These electrons are free to interact with the surrounding molecules thus increasing the adsorbing power of the graphene. This same phenomenon can be exploited in the use of electrodes and in catalysis.

Depending on the type of defect, other phenomena can arise to change the properties of the graphene. Below we indicate the main classified defects. [12]

The Stone-Wales defect is due to the transformation of four neighboring hexagons in the graphene structure into two pentagons and two heptagons maintaining the same number of carbon atoms and without the introduction of dangling bonds. It is a topological defect characteristic of carbon materials with sp^2 bonds. While being a two-dimensional defect, which remains in the plane of the graphene layer, its presence increases the probability of the graphene layer transforming into non-planar structures. Studies have been

done which report that the presence of Stone-Wales defects displaces atoms close to the defect itself from the plane, which in turn propagate this displacement [14]. The formation of such defect requires non-equilibrium conditions that provide the energy necessary for its formation. At room temperature it therefore needs external energy to form, but once formed, it is quite stable and requires some additional energy to return to the initial condition of pure graphene. The effect on the properties of graphene is due to the introduction of a shift of the Fermi energy in the band structure and a variation of the density of the states. These variations result in a change in the transport properties and increased reactivity of the carbon atoms that bind pentagons and heptagons. This latter property leads to the formation in these areas of more reactive adsorption sites for external molecules.

A single vacancy defect is due to the lack of a carbon atom in the graphene lattice with the formation of two rings, one composed of nine atoms and the other of five. Two of the dangling bonds join other atoms while one remains free, becoming the seat of a localized electron density, which leads to an increase in the adsorption capacity of single molecules. This defect needs a lot of energy to form and relatively less for the reverse transformation. From the point of view of properties, it is able to create a band gap in graphene, transforming it into a semiconductor . It can also give rise to ferromagnetic behavior [15]. Due to the low energy needed to eliminate the single vacancy, a carbon atom can easily move to fill the single vacancy causing a shift in the vacancy itself. Due to these movements, multiple vacancy defects can occur due to the contact of the single vacancy. Other types of structural defects can occur with the lack of more carbon atoms. If the defects are approached, they can create lines of defects that can be dominant in the transport characteristics of the graphene.

Another type of defect is due to the presence of a carbon atom external to the graphene layer which is positioned on the bond between two carbon atoms belonging to the graphene layer itself. A strong interaction is created between the carbon adatom and the neighboring atoms. It turns out to be a defect able to migrate easily on the graphene layer and in particular conditions it can favor the curvature of the graphene layer. [16]

Finally, the edges of the graphene layer can lead to the formation of line defects. In fact, the dangling bonds that are not passivated through the hydrogen bind to other carbon atoms giving rise to defects similar to those seen previously. This phenomenon is present both for graphene layers in armchair configuration and in those in zigzag configuration. [12]

2.5 Doping

Doping of graphene arouses much interest as it is possible to appropriately modify the electronic characteristics of the material. Pure graphene has no band gap, there is contact between the conduction and valence bands at the Dirac points, the Fermi energy level coincides with the energy level equal to zero. However, when a doping is carried out by replacing, for example, a carbon atom of graphene with an atom of another element, the

electronic band structure of the graphene layer is modified, and an energy gap can be formed between the bands of conduction and valence. Depending on the type of atom introduced, an n-type or p-type semiconductor graphene can be obtained. The Fermi energy level moves up the conduction band in the presence of a n-type graphene or moves down the valence band in the presence of a p-type graphene (Fig. 2.7). Many theoretical and experimental studies have been done to study the functionalization of graphene with the aim of obtaining the desired electronic characteristics for nanoelectronics devices and sensors. [12] [17] [18] [19]

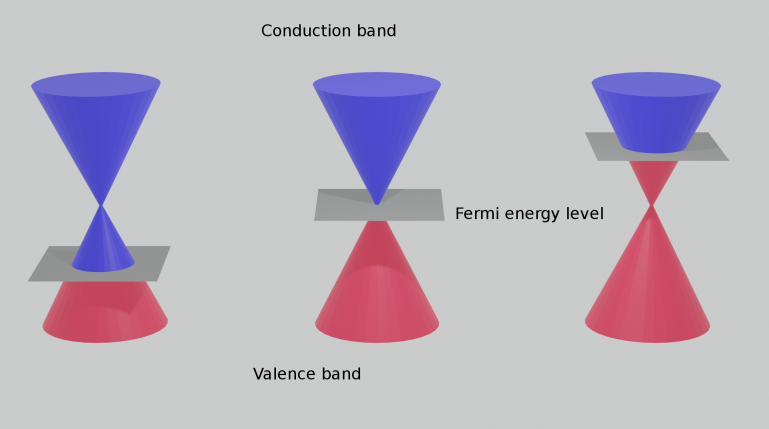

Figure 2.7: Band structure of graphene near the Dirac points; in the middle there is pure graphene; on the left there is graphene doped p-type; on the right there is graphene doped n-type

Several processes for obtaining doping of graphene have also been studied. There are two approaches that can be followed to obtain doping. The first is ex situ treatment in which the graphene is synthesized by itself and then the diffusion of external atoms on the graphene is carried out. This method allows a better control of the parameters related to the doping levels. For example, the replacement of graphene carbon atoms with atoms of other elements by bombarding graphene with high energy atoms and ions in a pulsed laser deposition chamber, forming vacancies and filling these vacancies with atoms of desired elements through dopant deposition. [18]

The second method is in situ treatment in which the synthesis of graphene is done directly together with the doping atoms.

The doping process is also important in sensing applications. In fact, the introduction of an impurity atom that replaces a carbon atom in the graphene layer can cause a charge transfer between that atom and the neighboring carbon atoms or vice versa. If the charge moves from the impurity atom to the graphene, the graphene results with a greater number of negative charges free to move and therefore a greater ability to attract external molecules to itself. In the same way, the doping atom can also become positively charged and be a possible adsorption site for the molecules.

Nitrogen, boron, phosphorus, oxygen and silicon are among the most studied doping

elements of graphene. For example, if a carbon atom in graphene is replaced with a nitrogen atom, an element which belongs to group 15 and to the p-block, a very electronegative element, in the periodic table, a greater interaction with external molecules can be obtained. In fact, the outermost electrons of nitrogen add to the delocalized electrons of carbon, leading to an increase in the negative charge and therefore a more probable strong interaction with any adsorbate. The key points are the difference in electronegativity between the carbon atoms and the dopant atom and the deformation of the graphene layer near the heteroatom with the formation of defects, caused for example by the different size of the atoms of different elements. These two characteristics lead to a change in the distribution of the local electron density with the formation of sites more suitable for the adsorption of the molecules. [12]

Chapter 3

Aflatoxin

Aflatoxins are a group of mycotoxins produced by fungi of the *Aspergillus flavus* and *Aspergillus parasiticus* species. They were discovered in 1960 in England following an outbreak that killed thousands of turkeys. To date there are almost twenty compounds that fall under the name of aflatoxin [20] but six are considered the main ones, the aflatoxins A1, B1, G1, G2, M1, M2. The letters B and G derive from the blue and green colors of fluorescence that aflatoxins emit when hit by ultraviolet light. The M instead, refer to milk, which is the first product in which they were detected and are hydroxylated metabolites produced by type B aflatoxins.

Among these the most widespread and dangerous is aflatoxin B1 (figures 3.1 and 3.2).

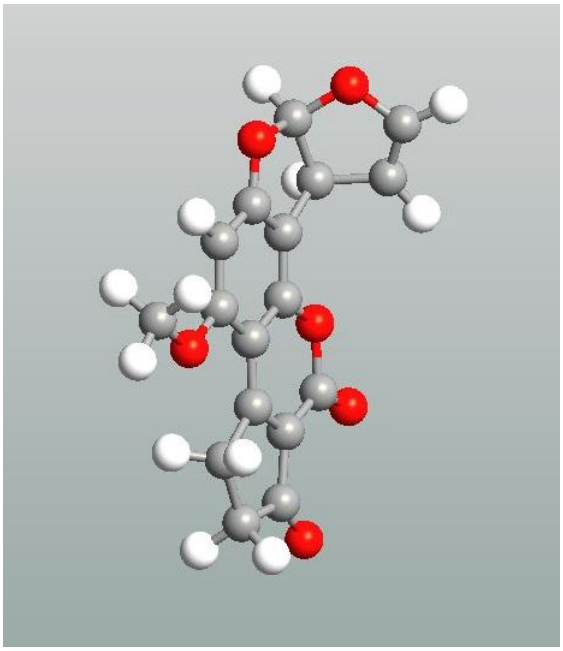

Figure 3.1: Aflatoxin B1 molecule

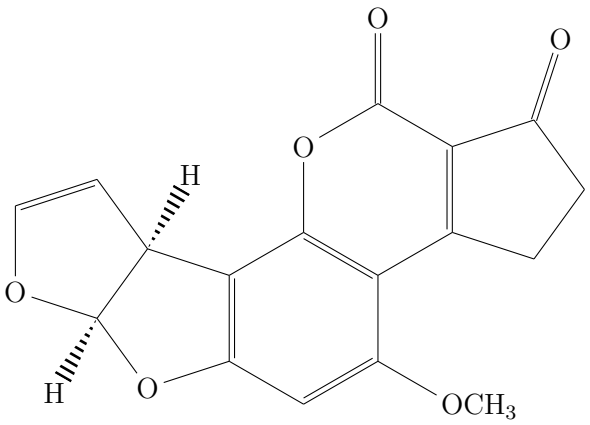

Figure 3.2: Structural formula of aflatoxin B1

Aflatoxins contaminate a large number of agricultural products such as corn, rice, cocoa beans, spices, nuts. The main causes of contamination are the use of inadequate agricultural practices that increase the contact of products with the soil, damage caused by insects to the surface of agricultural products and the storage of products in humid and unventilated conditions. Through these conditions there is an increase in the formation of fungi and molds from which aflatoxins can be produced. [20]

Another big problem is the presence of aflatoxins in animal feed. The concentration of aflatoxin increases along the production and marketing chain. Contaminated feed is ingested by animals. Aflatoxin B1 is transformed into its hydroxylated metabolite M1 which remains present in animal products such as milk. So, the consumption of milk and dairy products like cheeses then become dangerous for human health.[20]

Human exposure to aflatoxins derives mainly from the ingestion of contaminated food, even if one can be exposed to the risk of inhalation in closed places due to the presence of the molecule in the air. From a human health point of view the International Agency for Research on Cancer (IARC) has classified all four aflatoxins as group 1 carcinogens. M1 belongs to group 2 [21] [22] [23]. In particular Aflatoxins B1 is very dangerous substance that exhibit high toxicity for humans and animals with genotoxic, carcinogenic and immunosuppressive effects. It is highly mutagenic and carcinogenic, it is in fact able to bind to the bases of DNA, modifying them. The main organ involved in intoxication is the liver and depending on the type of exposure to aflatoxin, time and concentration, there may be acute toxicity (aflatoxicosis), edema, haemorrhagic necrosis of the liver, lethargy. Toxicity leads to hepatocellular damage and can result in acute hepatitis, fibrosis and other diseases. [24] [25]

In favorable climatic conditions, the spores of the *Aspergillus* fungus spread and are able to germinate, producing aflatoxins. Such conditions are hot, humid weather that favors the growth of mold and fungi, or extremely dry weather.[26] They are spread all over the world but due to their environmental conditions their presence is greater in African

and Asian countries, in tropical and subtropical climates. However, their presence is also growing in Europe, and in the coming years it could increase due to the ongoing climate change. Recent studies based on predictive models have documented the increase in their diffusion in Europe following a two-degree increase in average temperature, a scenario considered more likely for the next few years [27].

Therefore, due to its danger to humans and its widespread diffusion in various parts of the world, the monitoring and management of aflatoxins is increasingly important.

Chapter 4

Adsorption

A molecular gas sensor is a device whose properties change in the presence of a gas molecule, compared to the characteristics it possesses in the absence of that molecule. Due to the interaction of the molecule with the conductive channel of the device, a change of a specific quantity is obtained, for example the electrical conductivity through the device. For a change in device characteristics to occur there must be some interaction between the device channel and the gas molecule. It is therefore necessary to introduce the concept of adsorption, i.e., the process by which a connection is created between the gas molecule and the surface of the device. [12]

The adsorption process is due to the surface energy, a quantity that quantifies the breaking of the intermolecular bonds in the creation of a surface. In fact, the atoms on the surface are not completely surrounded by other atoms of the adsorbent but are free to interact with other atoms and molecules. The atoms on the surface have higher energy than those inside the solid and this excess energy constitutes the surface energy. Due to this lower stability due to the higher energy, the surfaces are not motionless zones but are ready to react through processes that reduce their energy such as passivation and adsorption phenomena.[28]

Adsorption is a process that only involves the surface of the device. The adsorbate (the gas molecule) binds to the surface of the material of which the sensor channel is composed through several possible chemical interactions. In the case where the interaction is the van der Waals forces or the presence of electric dipoles in the adsorbate, we have what is called physisorption, if the interaction is due to a covalent or ionic bond, we have a chemisorption. [28]

When it comes to adsorption, this process is divided into two categories, physisorption and chemisorption. In the first case we speak of physical adsorption because the interaction that takes place is of a physical, mechanical nature, while in chemical adsorption there is the formation of actual chemical bonds. The division between physisorption and chemisorption is not sharp and separate but there is a transition from one phenomenon to another. This gradual transition can occur differently depending on the chemical species involved. [29]

Physisorption or physical adsorption is an adsorption phenomenon mainly due to van der Waals forces. The effect of these forces is modified by additional electrostatic components such as polarization and field dipole which can be especially important in the adsorption of polar molecules. The interactions that take place between the two species are small, rapid and reversible. They mainly occur at low temperatures. There is no charge transfer, but they can cause a polarization of the adsorbed molecule. The adsorption energy is low and so is the heat released during its formation. In physisorption there is no directionality in the interactions between the adsorbed and the surface and therefore neither specific site of adsorption. Chemisorption is instead a phenomenon that leads to the formation of strong chemical, ionic and covalent bonds. Chemical bonds are directional, so the interactions that form between molecule and surface have a precise direction, orientation and position. Between the elements involved there is a strong sharing of the electronic charge or a strong transfer of the charge itself. It is usually a slow and irreversible process which can take place in a wide range of temperatures. During this process, a dissociation of the adsorbed species can also occur. The phenomenon leads to a total energy of the adsorbent plus adsorbed system decidedly lower than that given by the sum of the two isolated species, therefore during the formation a high increase in heat can be observed due to adsorption.[30]

The nature of the adsorbent surface is important, since in the presence of a non-polar surface the van der Waals forces are dominant, therefore the interaction with the molecule will be considerably influenced by characteristics such as the presence and size of pores on the surface or the size and polarizability of the adsorbed molecule. If the surface is composed, for example, of carbon atoms, it could oxidize and become partly polar. With a polar surface the interacting forces can become much larger. [30]

In chemistry, adsorption is measured through isotherms, which allow us to calculate the quantity of the molecule adsorbed on the adsorbent. Calculations are made at constant temperature and as a function of concentration or pressure. There are various models of isotherms including the first discovered and one of the most famous is that of Langmuir.

Adsorption energy is the energy released by the system during the adsorption process. Typical values for adsorption energy are 10 kJ/mol for physisorption and 120 kJ/mol for chemisorption. In general, we talk about physisorption with values $\leq$ 30 kJ/mol and chemisorption with values $\geq$ 100 kJ/mol. [28]. A resulting system with total energy less than the sum of the energies of the two starting isolated systems is a more stable system, the adsorption energy is negative. If the energy is negative and its absolute value is large, the stability of the system will be greater. Its value reflects the strength of adsorption. A positive value indicates a repulsive force and therefore an overall unstable system, while a negative value indicates that the overall system is more stable than the two individual isolated systems and the more negative the value, the stronger the adsorption is.

In the description of the adsorption process we can find ourselves faced with three situations, with all the possible intermediate variations. As we bring the molecule closer to the adsorbent surface, thus decreasing the distance, we can have:

- a weak chemical bond (van der Waals forces) which finds its minimum in adsorption

energy (maximum adsorption) at a certain distance between the two substances involved, the bond energy is small, as is the attractive force between them. As the distance decreases further, the force becomes repulsive. Instead, by increasing it, the attractive force slowly decreases.

- a strong chemical bond (ionic or covalent bond) is created between the two substances. Depending on the distance between the two substances, a global minimum is found for the energy of the system of large absolute value corresponding to a strong attractive force. Further decreasing the distance increases the repulsive forces.

- between the two substances, depending on the distance between them, a local minimum of energy is formed at a greater distance due to the phenomenon of physosorption. As the distance decreases, an energy barrier is encountered. The height of this barrier can vary from very high to zero. If this barrier is overcome by further decreasing the distance, a global minimum of energy is obtained due to the phenomenon of chemisorption. By further decreasing the distance, the repulsive forces dominate. The barrier can be overcome for example if the adsorbate molecule approaches the adsorbent surface with sufficient thermal energy to overcome the barrier and form a strong chemical bond. [31] [32] [28]

In general, the adsorption process changes according to the position of the molecule on the surface, i.e., the binding energy changes by moving the molecule from one site to another. This means that there is a potential barrier along the surface that the molecule must overcome in order to move from one location to another. If the temperature is high enough the adsorbate can have enough energy to move as a gas along the surface of the adsorbent. If the potential barrier is not uniform on the surface, zones of different diffusion of the molecules and the formation of adsorbed islands may occur. The adsorption of a molecule on a surface also depends on the kinetic energy with which the molecule arrives. If, for example, the speed is too high in contact with the surface, the interaction forces are not able to hold the adsorbate which therefore moves away. [28]

4.1 Adsorption on graphene

Graphene is a material capable of easily adsorbing external molecules, thanks to the sp^2 hybridized bonds which leave the electrons of the p_z orbitals basically free to bind to atoms and molecules outside the graphene layer. Its electronic properties are also sensitive to these molecules in the surrounding environment and is thus able to detect their presence. In fact, very often in the presence of a target molecule a change in its electronic and magnetic characteristics can be identified. This change is similar to that obtainable through doping of graphene itself. So high hopes are placed on this material for the design of future sensors sensitive to single molecules. Many studies have been done on the adsorption process of various types of molecules on graphene.

The adsorption of atoms and molecules on graphene can change depending on the orientation of the molecule relative to the graphene. But also based on the adsorption site

on the graphene: on the top of carbon atom, on the top of carbon-carbon bond or at the center of hexagon. The adsorption site is usually more important for smaller molecules. Studies carried out lead to the conclusion that in the case of physorption of molecules on graphene, the orientation of the molecule is important, less important is the adsorption site. The molecules also have a tendency to form clusters, which may be important when considering the concentration of the adsorbate. [33] [34]

Studies reveal that a strong change in graphene characteristics in the presence of an adsorbed can be obtained when new external electronic states are introduced. This can occur in the case of the formation of a covalent bond that changes the electronic structure of graphene with the formation of new electronic states. Or in the case of open shell molecules that have partially occupied valence orbitals and have electronic states with energy close to the Dirac point of graphene. In this case there is a charge transfer mechanism between the molecule and graphene. If the HOMO level (highest occupied molecular orbital) of the adsorbed is higher than the Dirac point of the graphene, electrons will flow from the adsorbed to the graphene. If the LUMO level (lowest unoccupied molecular orbital) is lower than the neutrality point of graphene, there will be a transfer of charge from the graphene to the molecule. This mechanism can also be used for the doping of graphene itself. Examples of this phenomenon have been presented with the NO_2 molecule.[33] [35]

In the presence of some molecules, pure graphene does not have large adsorption capacities. Examples are carbon monoxide and carbon dioxide, molecules responsible for air pollution and around which numerous studies have been carried out to identify them and limit their damage to the environment and humans. The CO molecule adsorbed on the pristine graphene causes a slight distortion of the graphene near the adsorption site, and the molecule in turn experiences a slight change in the length of its carbon-oxygen bond compared to that found in the isolated molecule. The adsorption energy is negative but small, indicating a weak physisorption process due to van der Waals forces. The final distance in stable configuration is about 3.5 Å. A similar trend is obtained for the CO_2 molecule. Instead, the analysis of the adsorption with respect to graphene with various types of doping shows higher adsorption values indicating the great potential of graphene functionalization. [36] [37]

Research have been done on the adsorption of different molecules on graphene, analyzing their characteristics and comparing them with those obtained with doped graphene. All this to find the best graphene structure for the single molecule. For example, the ethylene oxide molecule was investigated through density functional theory calculations, studying geometry optimization and absorption energy and carrying out various analyzes on pure graphene and on doped graphene silicon, aluminum, boron. The results obtained are better in the presence of aluminum doped graphene and with silicon doped graphene. Very often in research an improvement of the characteristics is obtained through some doping of the graphene compared to pure graphene. [38]

Chapter 5

Graphene sensor

The gas sensor is an electronic device capable of detecting gas molecules. Its operating principle is based on the change, in the channel, of one of its characteristics in the presence or absence of the gas molecule to be identified. The channel is an area of the sensor, the part sensitive to the gas molecule. These sensors can be of various types, based on the variation of different characteristics. The main properties of a good sensor are: high sensitivity, high selectivity, independence from temperature, low working temperature, rapid response, low consumption of adsorbed molecules. In particular for its particular characteristics, great interest is directed to sensors with a channel made of graphene.

Graphene thanks to its particular properties could be used in various applications of sensing. For example, as photoelectric sensors, thanks to its great transparency it can be used as photoconductive sensors or in photovoltaic cells; it can be used as a photodetector and for other applications because it is capable of absorbing a wide range of frequencies ranging from ultraviolet to terahertz. As electric field sensor, in which the density of graphene carriers is modified by the application of an electric field. As mechanical sensors in which a change in mass or strain detector can be detected; indeed, an asymmetric force applied to graphene is able to open a band gap and thus be detected with a sensor [39]. But also, magnetic field sensor, electrochemical sensors, and of course chemical sensors [40].

There are several methods of identifying molecules on graphene: change in electrical resistance and in electrical current but also changes in electrical resistivity frequency changes of surface acoustic waves. But most base their operation on the variation of graphene's conductivity in the presence or absence of the target molecule.[9]

For those sensors in which the sensing property is a variation of the conductivity, there are two main factors which lead to its variation, and therefore to the variation of the current: the concentration of charge carriers and the mobility of the carriers. Regarding the former, the adsorption of the molecule causes a variation of the charge carriers on the surface of the graphene and since the conductivity is proportional to the density of the charge carriers, a variation of the latter causes a variation of the conductivity. For the second, the conductivity is also proportional to the mobility, and therefore to the

scattering phenomena, with the adsorption of the molecule there could be an increase in scattering and a reduction in mobility.[41] [42] [9]

We know that graphene has a particular band structure which, for low energy levels, therefore near the neutrality points, has a linear trend. The adsorption of a molecule can create a doping of the graphene which will therefore lead to an increase in carriers, holes if it is an acceptor and electrons if it is a donor. For this reason, the ability of graphene as a gas sensor results highly sensitive towards different types of molecules.

There are various reasons why graphene is an excellent candidate for constituting the channel of a sensor.

1) It is composed of only carbon atoms; therefore, the valence electrons are not involved in chemical bonds and are free to interact with other molecules, suggesting good interactions with them. Indeed, being made from a planar layer of atoms with sp^2 hybridized bonds, the electrons belonging to the p_z orbitals perpendicular to the plane of the graphene are free to interact. Moreover, each atom of the structure can interact directly.

2) The operation of the graphene sensor is therefore based on the change of its electrical conductivity and therefore of its resistivity in the presence of the target molecule absorbed. When the target analyte is adsorbed on the graphene surface, there is a change in the concentration of local carriers in the graphene. The molecule acts as a charge donor or acceptor, there may be a transfer of charge between the molecule and the surface which leads to a change in the conductivity and therefore in the resistance of the sensor.

3) Since graphene is a planar set of carbon atoms linked together through covalent bonds and forming a planar layer of atoms, it is a two-dimensional crystal and therefore the contact surface between the adsorbate (molecule) and adsorbent (graphene) is maximized compared to the overall volume of graphene, i.e., there is a high surface/volume ratio. This means that the entire volume of graphene is exposed to the adsorbate presumably leading to a stronger and therefore more easily measurable response. The possibility of building arrays of such sensors leads to an increase in the available contact area between graphene and adsorbate, obtaining greater sensitivity for a reduced exposure time, which is very important especially in the presence of toxic gases, also present in low concentrations.

4) Through nano sensors made of graphene it is possible to identify individual gas molecules, which is not possible with traditional solid-state sensors. The sensitivity of graphene is due to its characteristic of being a material with low electronic noise which therefore makes it possible to detect changes even in the presence of single molecules. In fact, the high conductivity of graphene with a metallic conductance even with a charge density close to zero leads to a low noise even at the limit of absence of charge carriers. Furthermore, there is a low excess noise due to thermal switching thanks to the few defects usually present in graphene.

All of these features make graphene-based sensors ideal candidates for detecting single gas molecules with high sensitivity.[12]

It is important to underline the importance of the quality of the graphene layer. Fabrication techniques are continuously improving to achieve single layers of high-quality graphene. The presence of defects in fact changes its electronic structure and therefore its properties and performance.

Today it is essential to use software tools that allow you to evaluate the functionality and performance of a sensor before physically realizing it. Research and design via computer allow you to have economic and time advantages. Today, methods based on density functional theory (DFT) are very popular. However, some precautions must be followed in using this approach, especially with graphene. Some studies have revealed the importance of choosing the type of functional and the parameters to be used to take into due account the action of the van der Waals forces. For example, they are important in the adsorption processes on graphene, where changing combinations can lead to differences and errors in the calculation of distances or adsorption energies. [43], [44]

For example, a theoretical study was done on the use of a pristine graphene for the identification of propane and butane gas molecules. The starting materials were a layer of pristine armchair graphene nanoribbon and the molecules of propane and butane. Simulations were made with QuantumWise Atomistix ToolKit (ATK) software to investigate the possibility of graphene to detect molecules and the variation of the current in the sensor in the presence and absence of targets. Changes in the density of states, transmission spectrum and current were detected in the presence and absence of the molecule. Graphene was found to be very sensitive to the presence of gases and was able to detect their presence through the change in current compared to that obtained with pure graphene alone [45].

Theoretical studies have been done to investigate doped graphene as a single molecule sensor. It has been seen that if the doping molecules are open shell a strong doping is obtained and the molecule is a strong acceptor; the doping is instead weak in the presence of closed shell molecules [40], [46].

Part II

Part two

Chapter 6

Simulations: Methodology, computational methods

The idea of this thesis work is to investigate graphene as a possible material for the realization of a sensor for the aflatoxin B1 molecule. Being the first phase of research, the analyzes are done through the use of software tools for simulations.

Methodology

The methodology I followed in the analysis of graphene as a sensor for aflatoxin is composed by these steps:

- The choice of graphene as the constituent material of the channel has already been motivated in the previous chapters, due to its important electrical properties, adsorption capacity of external molecules and high sensitivity. The investigation of the pure material, if it leads to positive results, avoids further design and manufacturing steps such as doping, thus saving costs and time.
- I analyzed the adsorption process of the aflatoxin B1 molecule on the graphene layer. I investigated the adsorption energies of eight different geometric positions of AFB1 with respect to graphene, identifying the most stable configuration.
- The device type chosen for the simulations is a two-terminal device. For the analysis of the characteristics in the first phase of study, to see if the initial promises can be kept, it is better to consider the simplest device both in a simulation phase and in a possible real manufacturing phase. Also, in this case there is a costs and time saving. Only in a later step and perhaps to improve performance can a three-terminal device such as a transistor be used.
- I verified the sensitivity of the conductive channel to the target molecule. I analized the change of the density of states and of the transmission spectrum at equilibrium in the presence and in the absence of the adsorbed molecule. I checked the sensor's ability to detect the molecule by changing the current flowing through it in the

presence and absence of the analyte. I saw if that difference is big enough to be detected in eventual real device. I investigated the possible reasons for current reduction in the presence of AFB1.

- I verified the selectivity of the sensor, i.e., the ability to identify the target molecule and at the same time be inhibited in relation to the other molecules in the surrounding environment.

Computational methods

The software tool used in all simulations is QuantumWise ToolKit (ATK) software by Synopsys. It is a platform composed of a set of tools that integrate for modeling at the atomic scale. It has several simulation engines using for example Hamiltonians of the tight binding model or density functional theory (DFT). The latter is the methodology used in my simulations. It is widely used in general for *ab initio* electronic structure and atomistic calculations and allows to obtain an approximate but computationally efficient solution of the many-body problem.[47]

For the simulations of relaxation, optimization of the geometry and calculation of the total energy for the isolated graphene, the isolated molecules and the graphene plus molecule systems, the parameters indicated in the table (6.1) were used.

LCAO CALCULATOR	
LCAO Basis Set	Exchange correlation: GGA Functional: PBE van der Waals correction: Grimme DFT-D3 Pseudopotential: PeseudoDojo Basis set: Medium

Table 6.1: ATK-DFT Calculator settings for adsorption simulations

All other parameters have been left by default, unless otherwise indicated.

I chose the PseudoDojo pseudopotential with basis set Medium in order to balance the accuracy of the results with the computational time and the necessary RAM. Experimental tests based on the atoms of the elements of graphene and aflatoxin B1, carbon, hydrogen and oxygen, indicated PseudoDojo Medium a good compromise between these characteristics. [48] [49]

In the calculation of the total energy of the system composed of graphene and external molecule, I enabled the van der Waals correction Grimme D3 which allows to better take into account the van der Waals forces in the presence of the semi local exchange correlation functional (GGA and PBE). Furthermore I enabled counterpoise correction which allows to compensate the superposition error (BSSE) thus allowing to obtain a more correct value of the total energy of the system. [48]

The table (6.2) shows the parameters used in the equilibrium simulations, while in tables (6.3) and (6.4) there are those used for the calculations of the transmission spectra

and the device density of states. Finally, the table (6.5) shows the parameters used in the analysis of the IV curves.

LCAO CALCULATOR	
LCAO Basis Set	Exchange correlation: GGA Functional: PBE van der Waals correction: Grimme DFT-D3 Pseudopotential: PeseudoDojo Basis set: Medium
Numerical Accuracy	Density mesh cut-off: Default setting Occupation method: Fermi-Dirac Broadening: 1000 K k-points: [9.0,9.0,201.0] Å
Iteration Control	Default settings
Algorithm	Default settings
Contour Integral Parameter	Default settings
Poisson Solver	Solver Type: Conjugate gradient Boundary conditions: A direction: Dirichlet B direction: Periodic boundary condition C (transport) direction: Dirichlet
Electrode Parameters	Default settings

Table 6.2: ATK-DFT Calculator settings for equilibrium simulations

Unless otherwise indicated, these parameters were used for all the simulations so that the results were as comparable as possible.

In the simulations with the passivated graphene layer, in the Poisson Solver I set equal to Dirichlet all the boundary conditions to account for the passivation of the edges, while in the other simulations I assumed the graphene layer to continue to infinity in the transversal direction (B periodic).

As we will see later on in the study of selectivity, sometimes these parameters together with those of the IV curves have not led to convergence for some molecules other than AFB1, therefore there are no values in correspondence with some bias voltages.

Transmission Spectrum Analysis	
Energy range	E_1 = -1.5 eV E_2 = +1.5 eV Points: 301
k-point sampling	Density: $k_a = 27$ $k_b = 27$
Energy zero parameter	Average Fermi level
Infinitesimal	1e-06 eV
Self-energy calculator	Recursion

Table 6.3: ATK-DFT Transmission Spectrum settings

Device DOS Analysis	
Energy range	E_1 = -1.5 eV E_2 = +1.5 eV Points: 301
k-point sampling	Density: $k_a = 15$ $k_b = 15$
Contributions	All
Energy zero parameter	Average Fermi level
Infinitesimal	1e-06 eV
Self-energy calculator	Recursion

Table 6.4: ATK-DFT Device Density of States settings

IV curve Analysis	
Energy range	E_1 = -1.5 eV E_2 = +1.5 eV Points: 301
k-point sampling	Density: $k_a = 15$ $k_b = 15$
Infinitesimal	1e-06 eV

Table 6.5: ATK-DFT IV curve settings

Chapter 7

Simulations: Aflatoxin adsorption on graphene

7.1 Adsorption: Simulation results and analysis

In this chapter I present the analysis and the results obtained regarding the adsorption process of the aflatoxin B1 molecule on a graphene layer. The graphene layer used for the simulations is shown in the figure (7.1) and is a rectangle of 40 hexagons (8 hexagons x 5 hexagons). I chose this size because AFB1 could be adsorbed in any rotation without going outside the edges of the graphene.

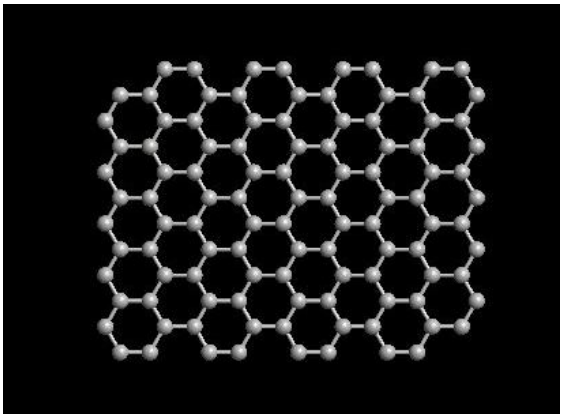

Figure 7.1: Graphene layer used for the adsorption processof AFB1

I rotated AFB1 in eight different geometric positions relative to the graphene. They have been chosen so as to bring the greatest number of atoms of the molecule closer to the graphene layer. The figure (7.2) shows the eight configurations studied. Configurations 2 and 4 differ respectively from 1 and 3 for a rotation of the aflatoxin of 90^{o} degrees in the graphene plane.

In all configurations, I placed the AFB1 at an initial minimum distance of about 2 Å

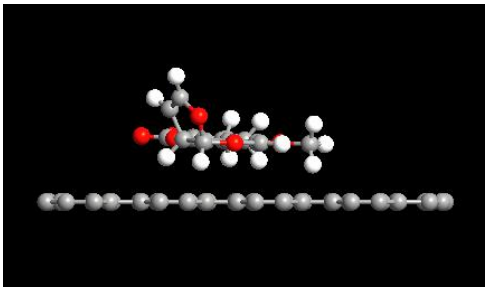

(a) Configuration 1

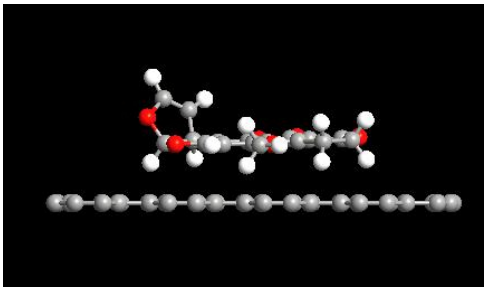

(b) Configuration 2

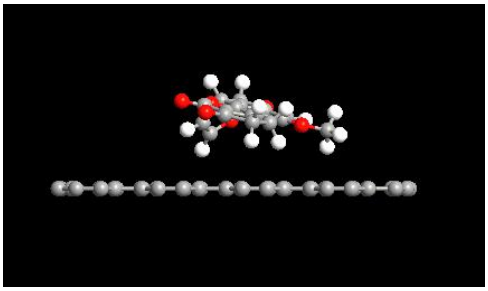

(c) Configuration 3

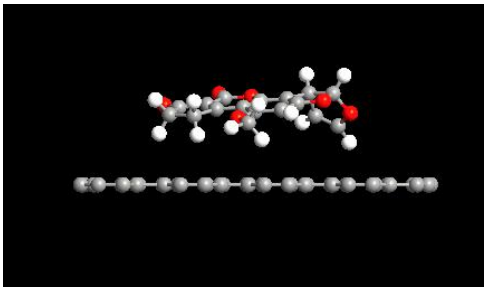

(d) Configuration 4

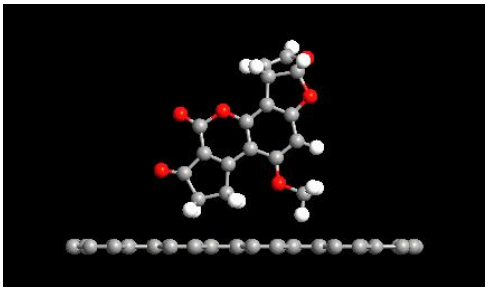

(e) Configuration 5

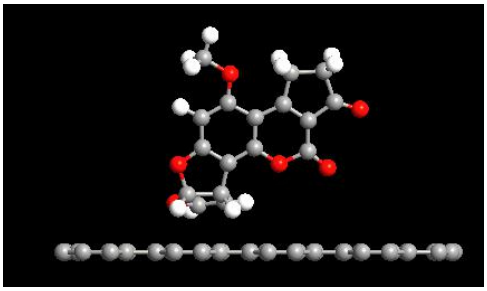

(f) Configuration 6

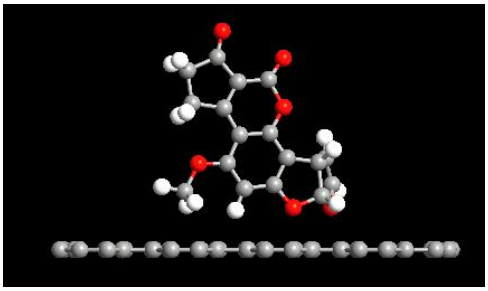

(g) Configuration 7

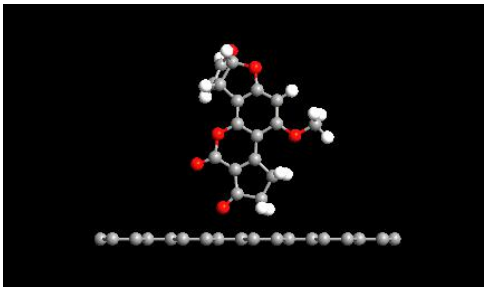

(h) Configuration 8

Figure 7.2: Configurations studied for the adsorption of aflatoxin on graphene

from the graphene. Then I allowed the system to relax unconstrained to reach the most stable configuration.

During the relaxation process, there was a gradual arrangement of the various atoms. In all eight configurations the final minimum distance was greater than the initial minimum distance (about 2 Å). This indicates that at 2 Å the repulsive forces were greater than the van der Waals interaction forces. The configuration 1, the one which, as we will see later, will turn out to be the most stable, we have a final minimum distance between graphene and aflatoxin of 2.77 Å (figure 7.3).

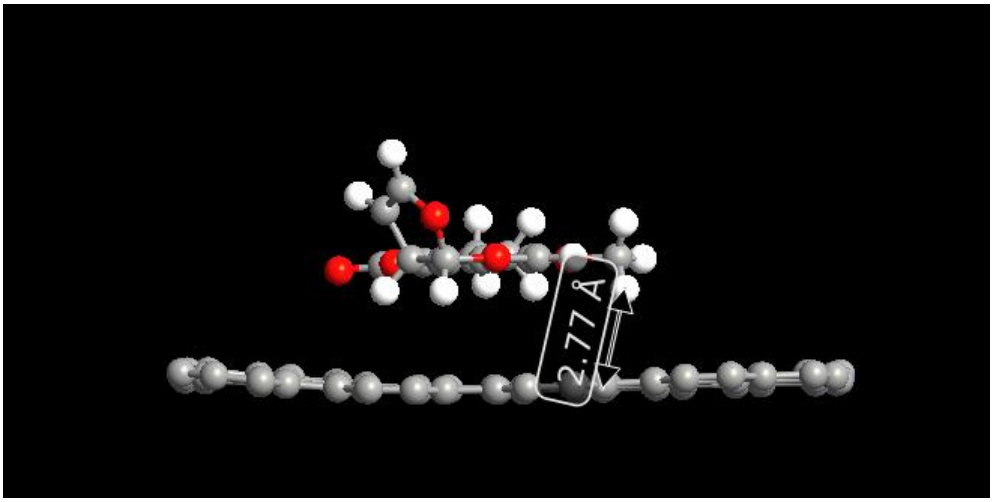

Figure 7.3: Minimum distance between graphene and aflatoxin atoms after the relaxation process of the system geometry for configuration 1.

Adsorption Energy

The adsorption energy, as explained in chapter 4, is the energy that is obtained during the process of adsorption of a molecule onto a surface. The resulting system (graphene + aflatoxin) is stable if the adsorption energy is negative, i.e., if the total energy of the final system is less than the sum of the energies of the two starting isolated systems. The final system is more stable if the adsorption energy is more negative (negative and in larger modulus). Into formulas:

$$E_{ADS} = E_{GR+AFB1} - (E_{GR} + E_{AFB1}) \tag{7.1}$$

where:

- $E_{GR+AFB1}$ is the total energy of the system composed of the graphene which has adsorbed the aflatoxin.
- E_{GR} is the total energy of isolated graphene.
- E_{AFB1} is the total energy of isolated aflatoxin.

The table (7.1) shows the adsorption energies of the eight configurations calculated through the equation (7.1).

Configuration	$\mathbf{E_{ADS}}$ **(kJ/mol)**
1	-112.4508
2	-109.9585
3	-103.6685
4	-102.8059
5	-32.3996
6	-46.7020
7	-48.8199
8	-32.5058

Table 7.1: Adsorption energies of the eight configurations

We can see that all the studied configurations have negative adsorption energy and therefore they are all stable configurations. However, the first four have much higher energy in modulus than the last four. The first four have the largest number of aflatoxin atoms that are able to interact with the carbon atoms of graphene. For these four configurations the modulus energy exceeds 100 kJ/mol , so there is a good interaction force between aflatoxin and graphene in these cases. Configuration 1 is the most stable with an adsorption energy of -112.4508 kJ/mol. The two most stable configurations will be used in the next chapter for the simulations in which I will investigate the characteristics of the sensor. I have decided to study the second one in addition because the energies

are similar. In the real case any perturbation in the ambient could allow the molecule to move and be absorbed in one or the other configuration.

Before moving on to the device, I did a further study regarding the adsorption site of aflatoxin on graphene, to see its influence on the adsorption energy. I took configuration 1, the most stable one and I moved the aflatoxin to three different graphene sites. The three sites on graphene are identified with the letters A, B, C:

A: above a carbon atom

B: above a bond between two carbon atoms.

C: on the center of a hexagon

and they are shown in the picture (7.4).

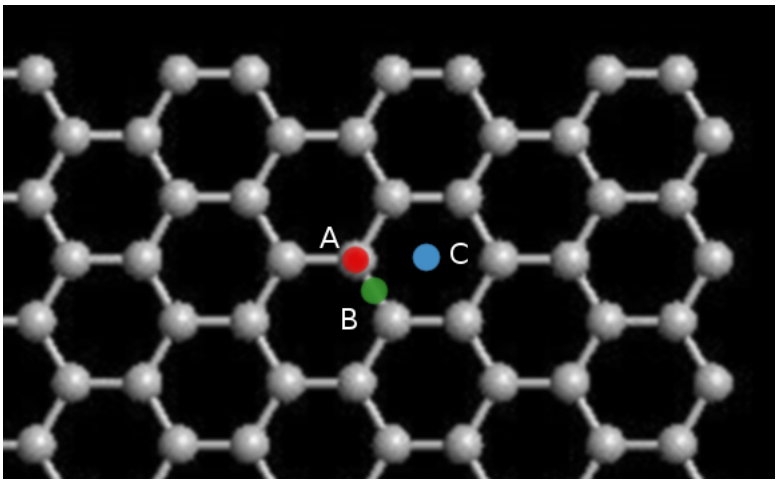

Figure 7.4: Adsorption sites

As can be seen from the results shown in the table (7.2), there is not a significant variation in the adsorption energy with respect to the adsorption site. The variation between the three positions is negligible.

Configuration	$\mathbf{E_{ADS}}$ **(kJ/mol)**
A	-112.4508
B	-112.4961
C	-111.8989

Table 7.2: Adsorption energies relative to the adsorption site

In conclusion I can say that the aflatoxin molecule binds to graphene. In four of the configurations analyzed, the interactions are quite strong. The adsorption energy strongly depends on the relative orientation between AFB1 and graphene while it is almost independent of the adsorption site.

Chapter 8

Simulations: Graphene sensor device

8.1 Sensor: Simulation results and analysis

For the study of transport phenomena, I used a larger graphene layer composed of 91 hexagons, 7 along the transversal direction and 13 along the transport direction. This is to keep the aflatoxin as far away as possible from the influence of the edges of the graphene and to keep the aflatoxin away from the electrodes in the transport direction. I have left a certain margin of safety (a certain distance) in these directions increasing the number of atoms in graphene. But I did not increment more to not increase too much the computational times and RAM memory occupation.

Before starting the transport simulations, I relaxed the geometry of the system graphene plus aflatoxin. I apply this to all the configurations analyzed below.

8.1.1 Configuration 1

The first configuration studied corresponds to configuration 1 of adsorption of aflatoxin on graphene, i.e., the one with the highest adsorption energy, i.e., the one most likely to be obtained during the adsorption phenomenon. The device used for the simulations is shown in the figure (8.1) in its perspective view, in the figure (8.2) in its front view, and in figure (8.3) in its view from above. In the latter figure the graphene layer is represented using the stick model in order to highlight the aflatoxin molecule.

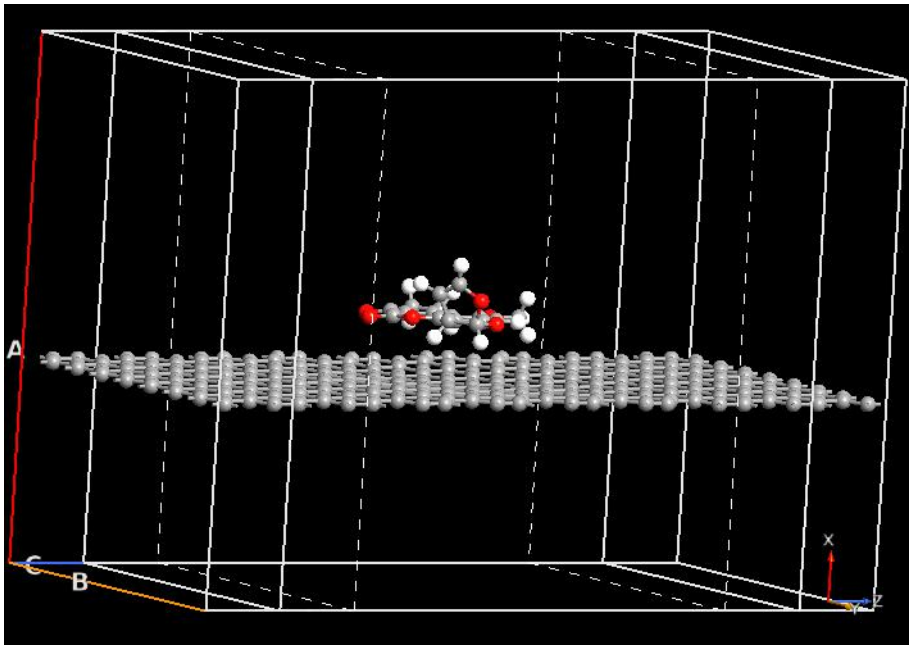

Figure 8.1: Device used for simulation with aflatoxin in configuration 1. View: perspective.

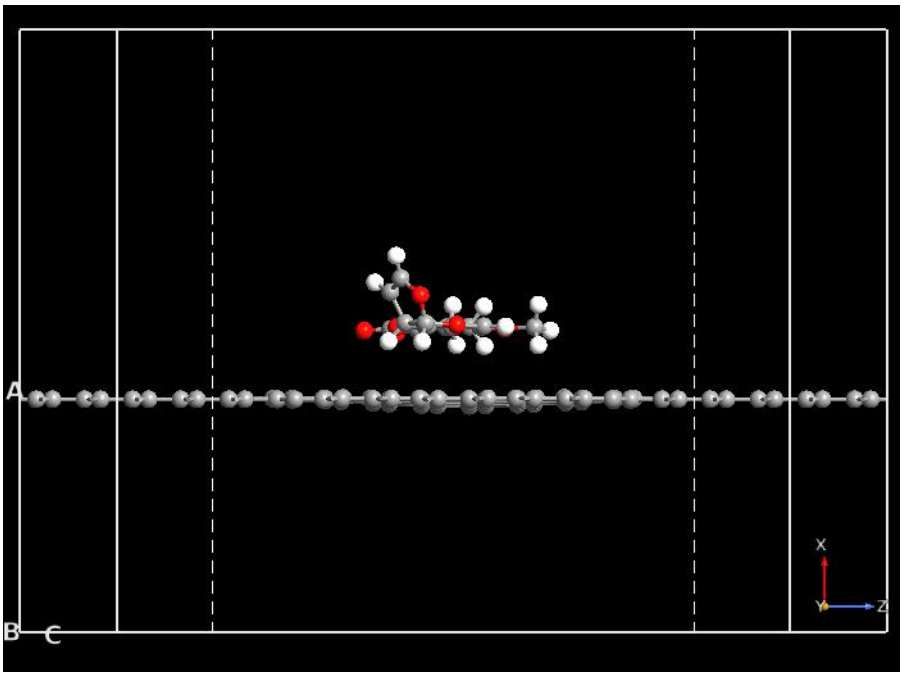

Figure 8.2: Device used for simulation with aflatoxin in configuration 1. View: front.

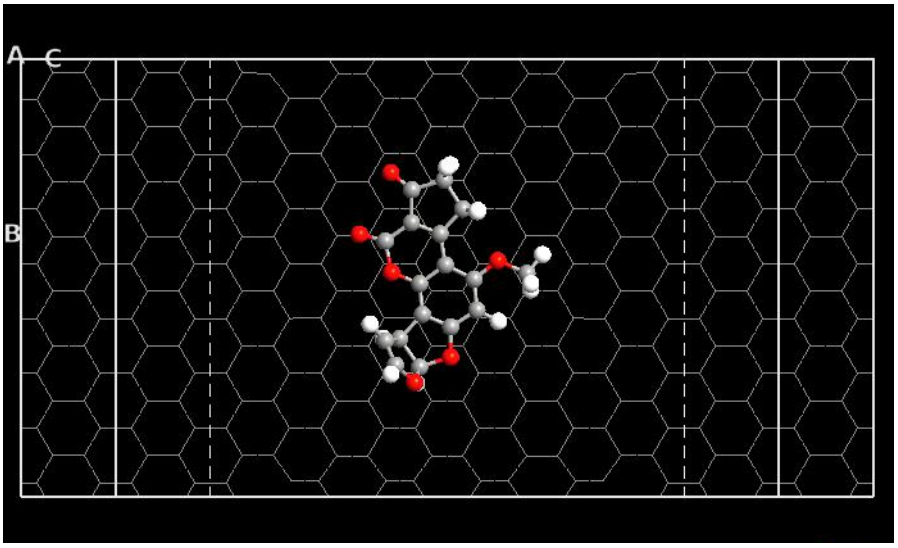

Figure 8.3: Device used for simulation with aflatoxin in configuration 1. View: from above.

After analyzing the adsorption of aflatoxin on graphene and concluding that a good interaction force is formed between them, I need to see if the molecule will be identifiable in the sensor. To do this I begin to analyze the density of states and the transmission spectrum.

Figure (8.4) shows the device density of states of graphene with (a) and without (b) aflatoxin. Note the difference between the two graphs. The presence of aflatoxin results in a change in the electronic states of graphene. We note the introduction of two peaks with negative energy at about -1.1 eV and -1.2 eV and a lowering of the peak that the DOS of graphene alone had at about 1.4 eV.

The transmission spectrum of the device allows us to analyze the contributions to the total transmission of charge carriers for different energy values. As can be seen from Figure (8.24), there is a change in these spectra in the presence and absence of aflatoxin. So, we expect that somewhere in the bias voltage there is a current difference between the device with and without AFB1.

In the analysis of the transmission spectra, I also went to see the contribution of HOMO and LUMO of aflatoxin. In figure (2.6) the HOMO and LUMO values can be seen in red, the transmission spectrum of the device in blue with the ideal graphene layer, not relaxed, i.e., it is not given the possibility to change the distances between its atoms during the phase of relaxation with AFB1 and in black the transmission spectrum of the device with the relaxed graphene layer. It can be seen that the peaks in the transmission spectra correspond to HOMO and LUMO of AFB1. The only unmatched peak is seen in relaxed graphene at about 0.8 eV. Such peak is not present in ideal graphene, so I assume it is due to the change in distance between atoms in the relaxation phase as it is not present if the graphene layer remains ideal.

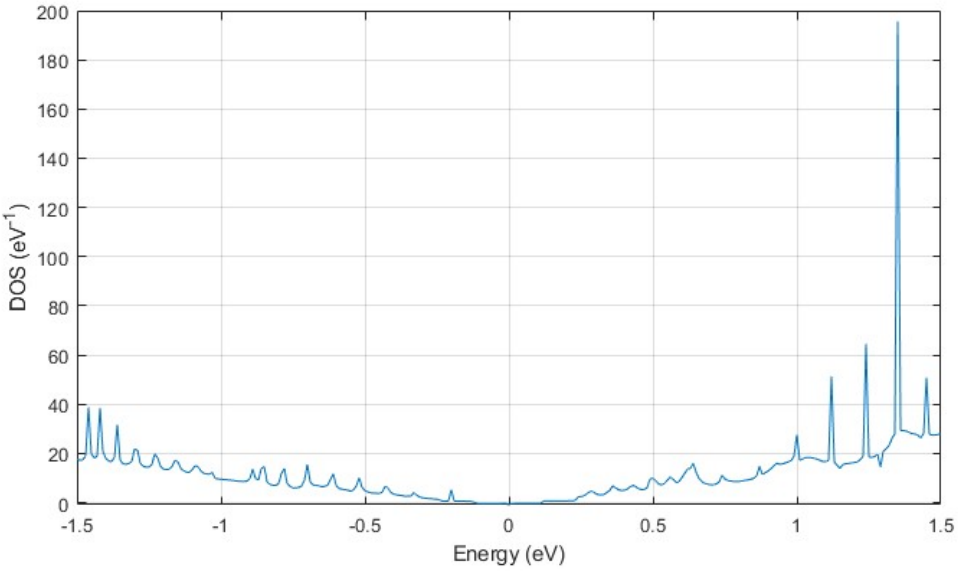

(a) Device Density of states of graphene without aflatoxin

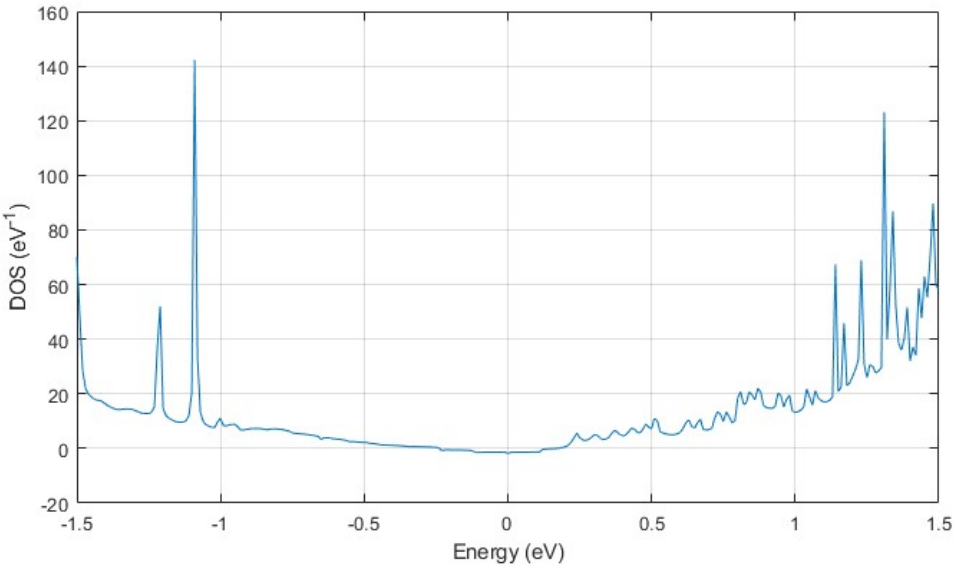

(b) Device Density of states of graphene with aflatoxin

Figure 8.4: Device Density of states

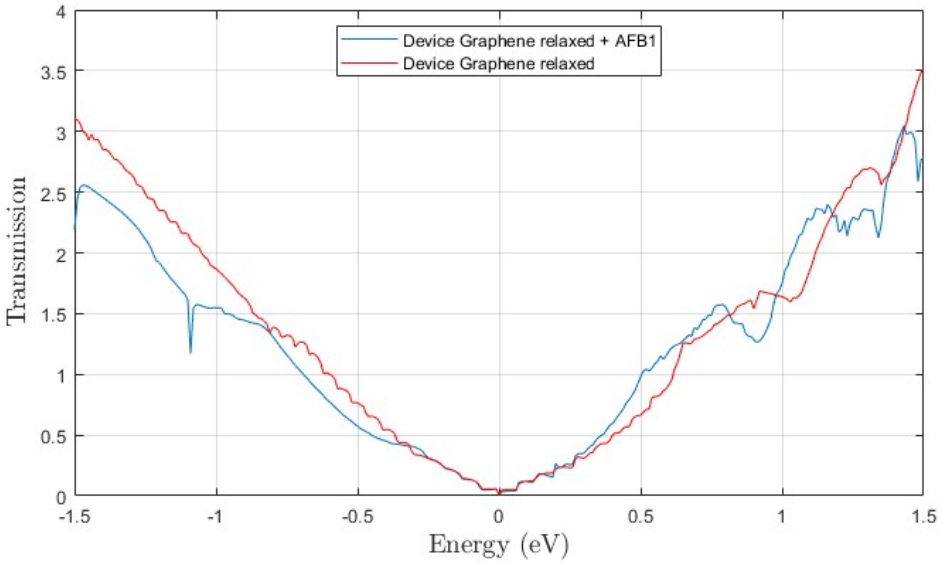

Figure 8.5: Comparison of equilibrium transmission spectra as a function of energy between graphene with aflatoxin and graphene alone

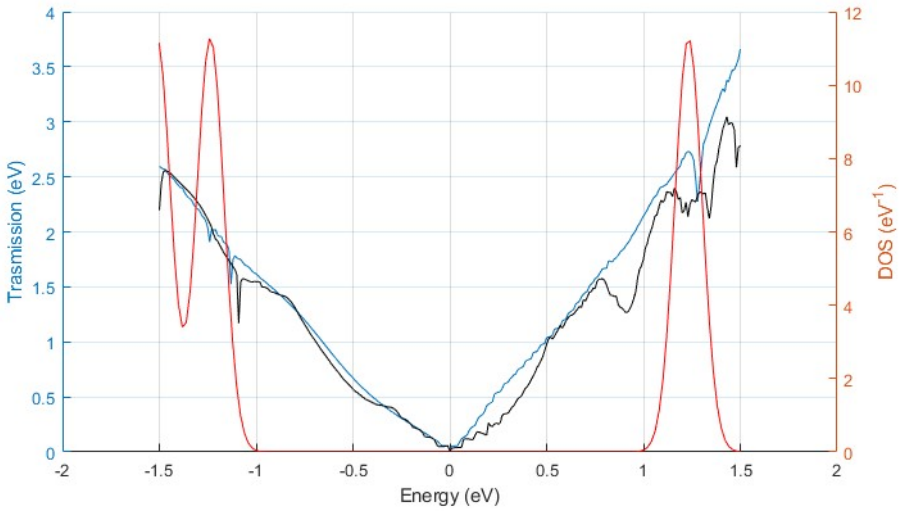

Figure 8.6: Comparison between Transmission Spectrum of ideal graphene device + AFB1 in blue, Transmission Spectrum of relaxed graphene device + AFB1 in black and DOS of AFB1 in red, where the two peaks HOMO and LUMO of AFB1.

The figure (8.7) shows the I-V characteristics of the sensor in the absence and in the presence of AFB1 in configuration 1. The two currents are different in some bias points taken into consideration.

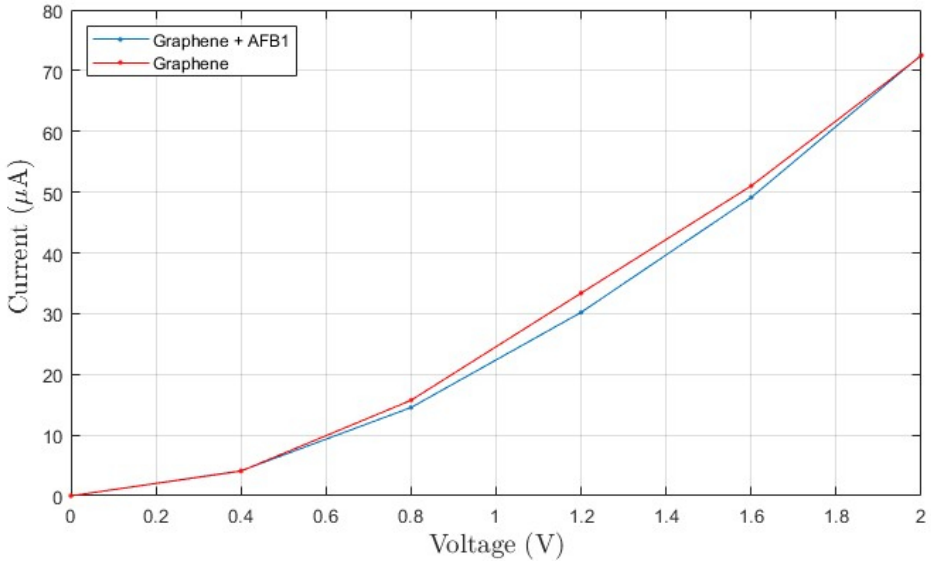

Figure 8.7: Comparison between the current in the graphene and the current in the graphene + AFB1 in configuration 1

The figure (8.8) shows the current difference value between the sensor in the absence and in the presence of AFB1 in configuration 1. The current variation is evaluated using the formula:

$$\Delta I_D = I_{D,GR} - I_{D,GR+AFB1} \tag{8.1}$$

while for the percentage variation of the current I use the formula:

$$\Delta I_{D\%} = [(I_{D,GR} - I_{D,GR+AFB1})/I_{D,GR+AFB1}] \cdot 100 \tag{8.2}$$

where $I_{D,GR}$ indicates the current in the graphene without aflatoxin and $I_{D,GR+AFB1}$ the current in the graphene sensor with the presence of aflatoxin. Therefore, a positive/negative value of ΔI_D corresponds to a decrease/increase of the current due to the presence of aflatoxin. A positive value indicates an increase in current in the absence of AFB1 compared to the value with the presence of AFB1. Therefore, as can be seen in correspondence with the simulated voltage values, the sensor with aflatoxin mainly leads to a reduction in the transmitted current.

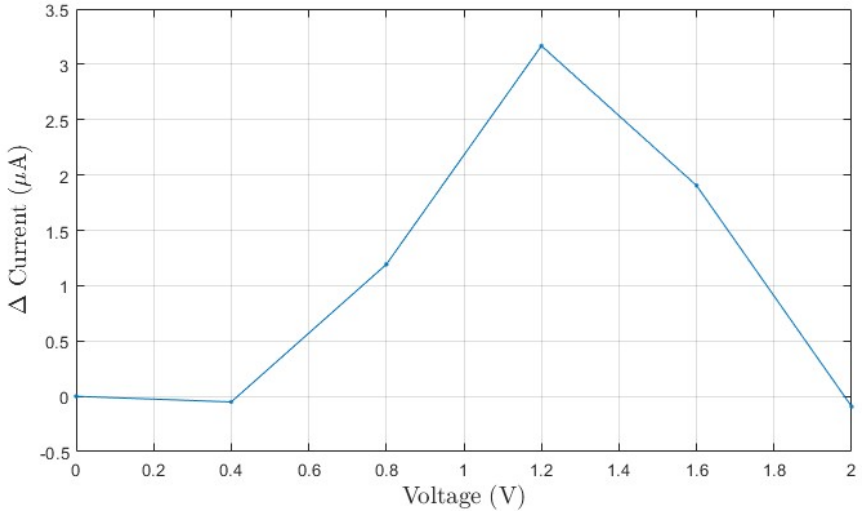

(a)

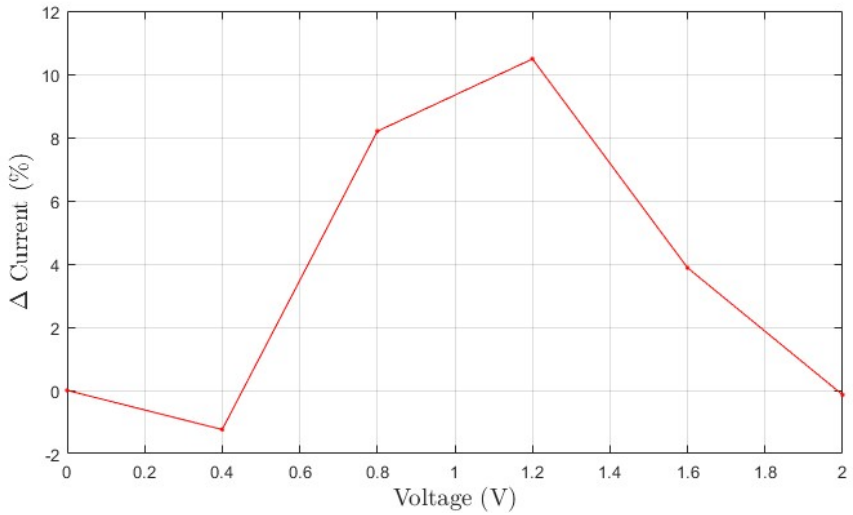

(b)

Figure 8.8: (a) Current variation (ΔI_D) in graphene and graphene + aflatoxin in configuration 1; (b) Percentage of current variation ($\Delta I_{D\%}$) in graphene and graphene + aflatoxin in configuration 1.

The response of the sensor depends on the value of the applied voltage. In the presence of aflatoxin, we obtain a reduction of the current for the bias points 0.8 V, 1.2 V and 1.6 V. There is a peak in the current difference in correspondence with the voltage of 1.2 V. That means there is a high sensitivity of the sensor to aflatoxin in this bias point. The corresponding current difference value is 3.167 µA. From the analysis of the percentage variation of the current, a maximum percentage variation of 10,48 % can be seen, always

in correspondence with the voltage value of 1.2 V. This bias value has the greatest current difference both in absolute value and in percentage, obtaining the best response from the sensor. It is the point of greatest sensitivity. Both the voltage of 1.2 V and the current difference of 3.167 µA are measurable values and compatible with the operation of an electronic device. In general, in a real device, in the final choice of the bias voltage for a sensor must also be taken into account the selectivity of the sensor. The selectivity could be higher at other bias points. In the sequel we will analyze the problem of selectivity.

Figure (8.9) shows the difference between the transmission spectra at 1.2 V of the device with and without aflatoxin. We can see that the transmission spectrum of graphene alone varies across jumps as the energy varies. This is because as the energy increases, the modes involved in the conduction increase. When a new mode occurs, there is an increase in transmission by a fixed amount. As we know from the theory recalled in chapter 2, the number of modes depends linearly on the energy. Same thing for the density of states. The DOS in graphene also grows linearly with energy, unlike materials with a parabolic dispersion relationship where the DOS remains constant. In this figure we can see within the bias window the transmission spectrum is larger in the absence of the molecule, resulting in a higher current.

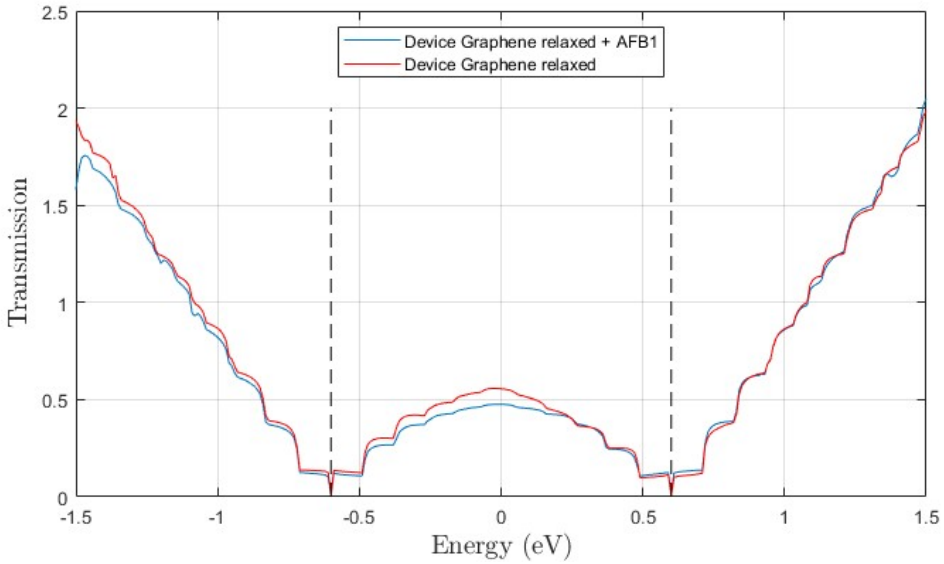

Figure 8.9: Transmission spectrum of the device with and without AFB1 at the bias voltage of 1.2V

The current in graphene depends on the conductivity of the charge carriers, therefore on their number and their mobility. The reduction of the current in the presence of AFB1 can be due either to a transfer of charge between the molecule and graphene or to scattering phenomena which decrease the transmission. To better understand the mechanisms that lead to the reduction of current in the presence of the molecule some other analyses have been done.

From the Projected device density of states, calculated at 1.2 V bias voltage, the localization of the electrons in the aflatoxin molecule can be deduced. In the PDDOS (figure 8.10) there are narrow peaks at determined energy levels, corresponding to the available states.

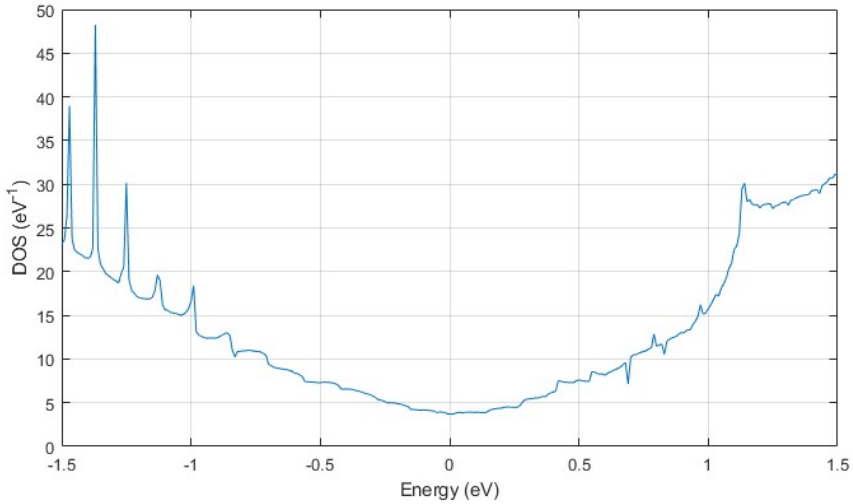

(a) PDDOS only graphene

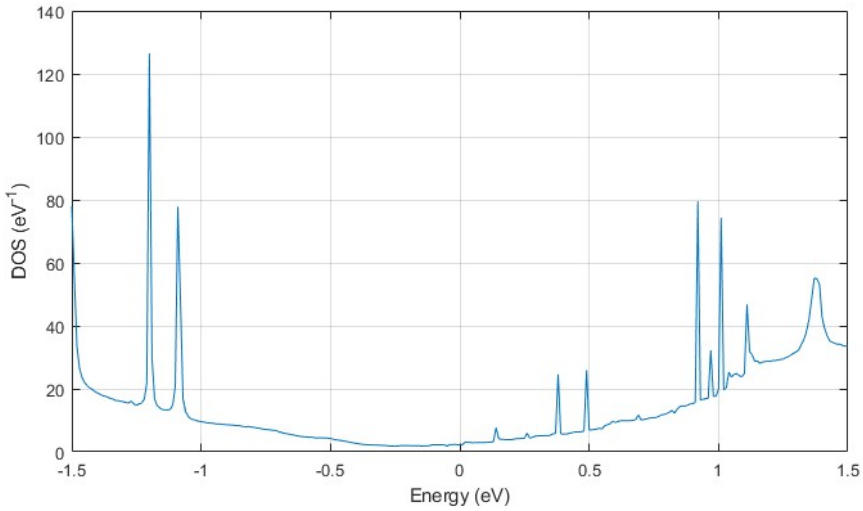

(b) PDDOS graphene + AFB1

Figure 8.10: Projected Device Density of States at 1.2 V bias voltage.

The little broadening (widening of states with respect to energy) indicates that the electrons remain in that state for a long period of time, therefore they have a long intrinsic time. Energy and time are linked by an uncertainty relationship, the greater the persistent time, the smaller the energy broadening will be. This indicates a localization of the

electrons. Localization also confirmed through the Electron localization function which, as can be seen in the figure (8.11), highlights the electrons located on the molecule without delocalization on the graphene layer.

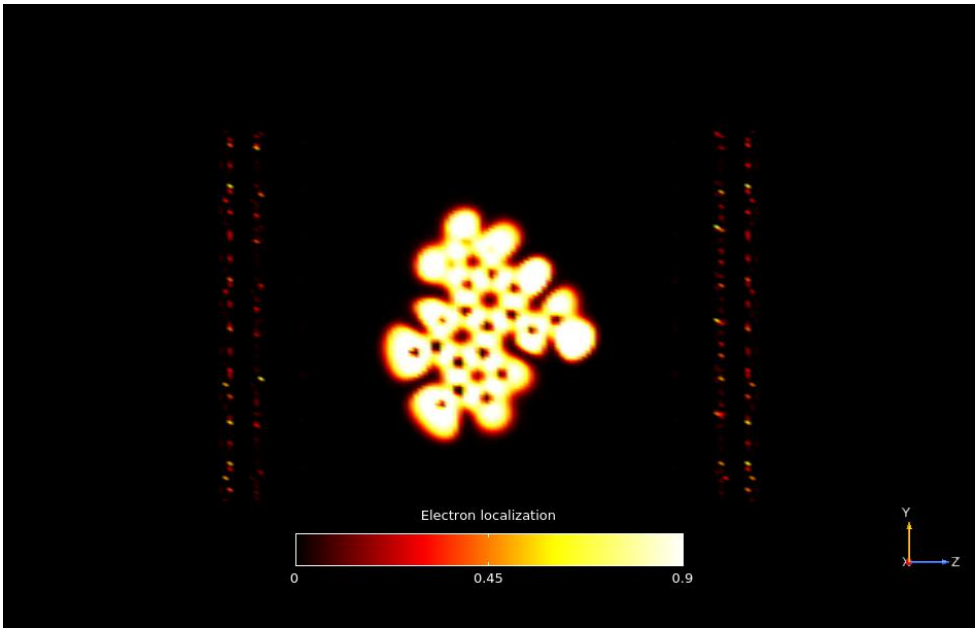

(a) View from above

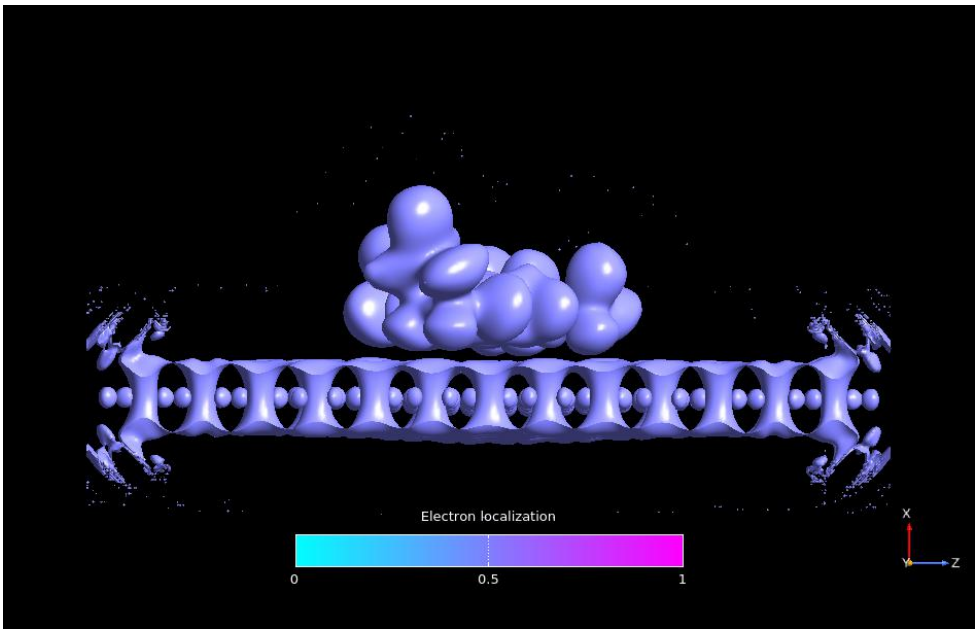

(b) Front view

Figure 8.11: Electron localization function

Through the analysis of the transmission pathways, the paths made by the electrons during transmission can be evaluated. In the figure (8.12) they are represented in the device with graphene alone (a) and with the presence of aflatoxin (b).

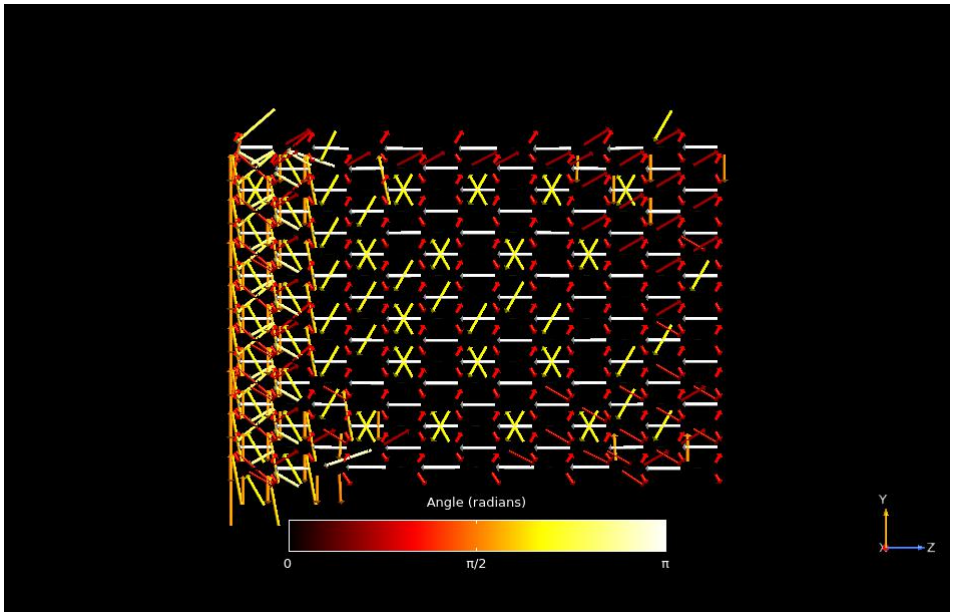

(a) Transmission Pathways with graphene only

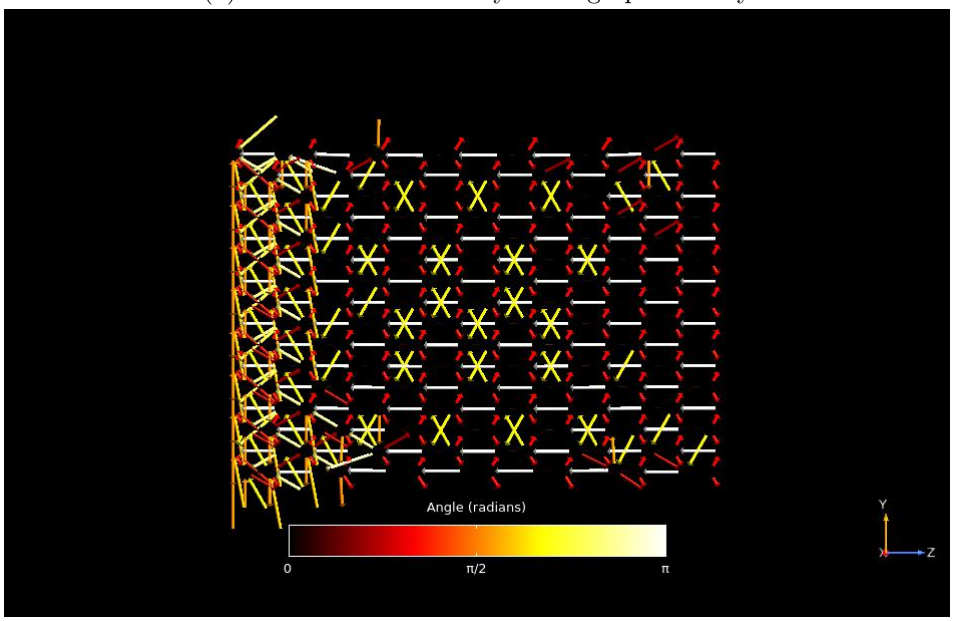

(b) Transmission Pathways with graphene and aflatoxin

Figure 8.12: Transmission Pathways

Arrows indicate the direction of electron transmission from one atomic site to adjacent ones, and their size indicates the magnitude of that transmission. As can be seen, in correspondence with the positioning of the molecule there are yellow arrows that go back to the left, in the opposite direction to the transmission. These arrows are not present in the graphene-only device. This indicates back reflections in the electron path that could explain the current reduction.

Finally, figure (8.13) shows the eigenstates related to transmission in the presence of AFB1. The very light areas near the aflatoxin towards the left of the device indicate the reflection of the transmission of part of the carriers. It is therefore presumable that scattering phenomena are present around the molecule.

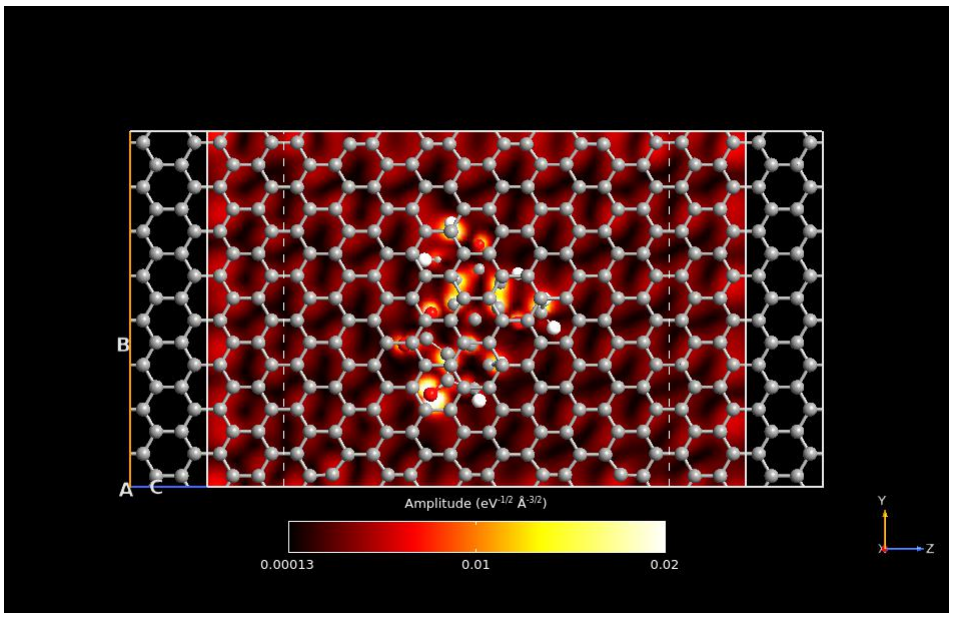

Figure 8.13: Eigenstates of device graphene + AFB1

Concluding these analyses, I can deduce that aflatoxin behaves as a scattering centre, a "scatterer", which introduces reflection phenomena probably due to the phase breakdown of the electrons which are transmitted from source to drain. Here I have considered only coherent transport so nothing can be said about inelastic scattering, related to incoherent transport and dissipative phenomena. The reason for this scattering can be an electronic repulsion between graphene orbitals and AFB1 orbitals. In other words it can be seen as a steric modification (i.e. a modification of the electronic properties of graphene, of its orbitals), which, breaking the periodicity of the electronic states of graphene (because a spatial modification of the orbitals is a modification of their spatial periodicity), decreases the transmission; like a crystalline defect in a periodic lattice, therefore behaves just like a scattering center. Hence the reduction of the current in the presence of AFB1.

8.1.2 Configuration 2

As previously done with configuration 1 of aflatoxin B1, I studied the trend of the current also in correspondence with configuration 2 of aflatoxin, different from the first due to a 90° degrees rotation of the molecule in the graphene layer. Its adsorption energy is comparable with that of configuration 1.

The trend of the current is very similar to that obtained with the first configuration. Figure (8.14) shows the current with aflatoxin in configuration 2 compared to the current with graphene alone.

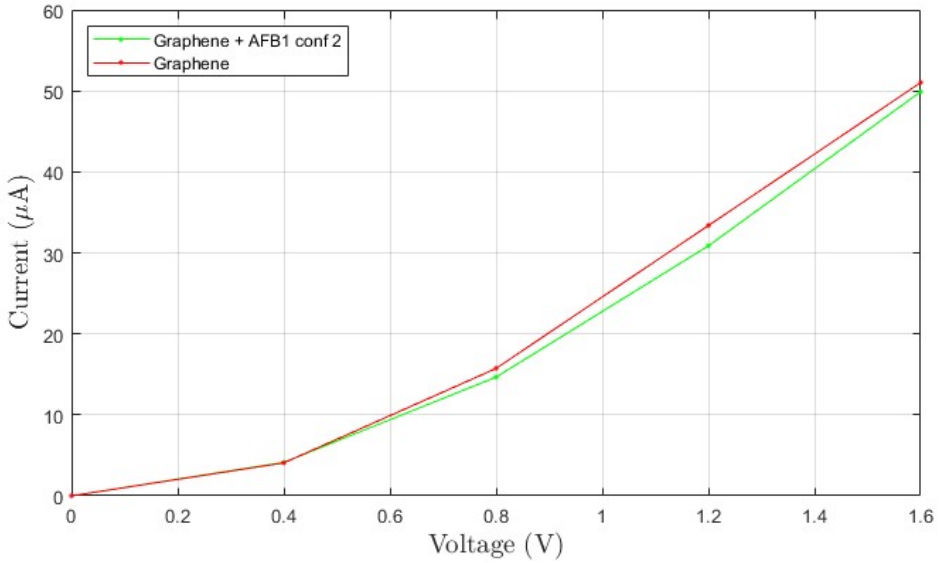

Figure 8.14: Current in graphene and in graphene + aflatoxin in configuration 2.

While in figure (8.15) the three currents are compared: graphene only, graphene plus aflatoxin in configuration 1 and graphene plus aflatoxin in configuration 2. In configuration 2 the current is generally slightly higher than that in configuration 1, but the difference is small. At a voltage of 1.2 V, the current in the second configuration is 0,656 µA greater than that in the first configuration. This bias point (1.2 V) is also confirmed for this second configuration as the point of greatest sensitivity for the aflatoxin B1 molecule. In figure (8.16) the area around 1.2 V is magnified. This similar current trend in the presence of the two AFB1 configurations is positive as it would facilitate the front-end electronic design phase of the sensor.

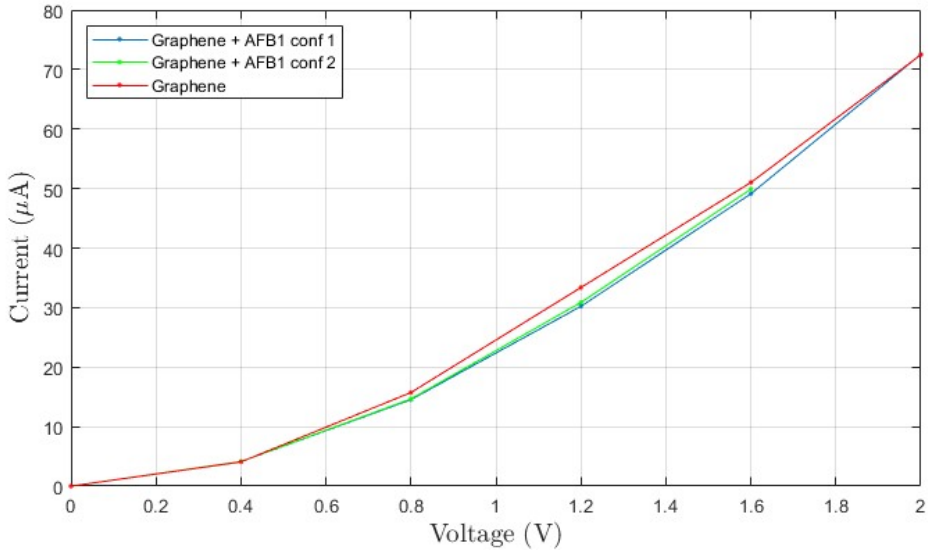

Figure 8.15: Current in graphene, in graphene + aflatoxin in configuration 1 and in graphene + aflatoxin in configuration 2.

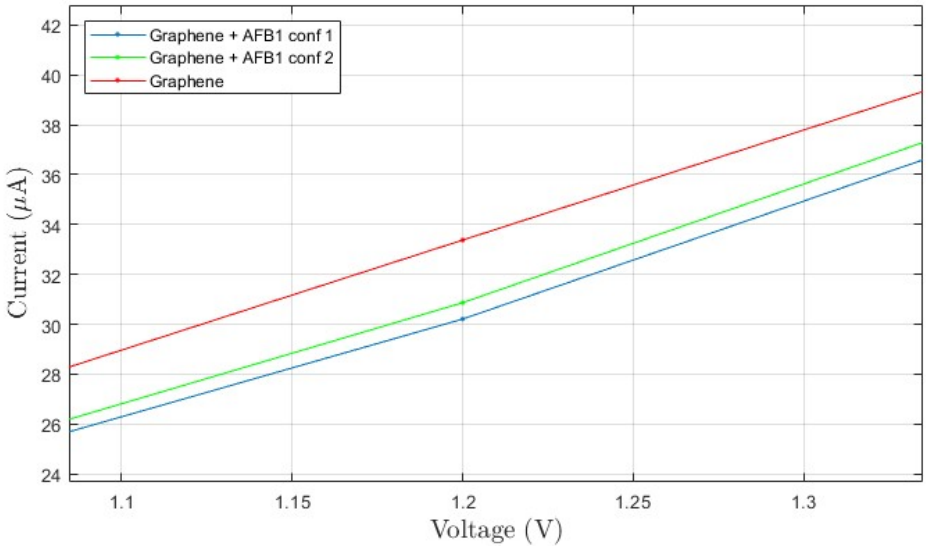

Figure 8.16: Zoom around 1.2 V of current in graphene, in graphene + aflatoxin in configuration 1 and in graphene + aflatoxin in configuration 2.

8.1.3 Passivated nanoribbon

After studying the adsorption of aflatoxin on graphene and having established that graphene is able to bind to the AFB1 molecule in a stable way and having identified the geometric configuration that maximizes the adsorption energy, I proceeded to study the transport properties in order to understand if a graphene sensor was able to detect AFB1. From what it has been seen previously, such a sensor is able to perform this task. The graphene layer used in the previous simulations had periodic boundary conditions transverse to the transport direction in the plane of deposition of the layer itself. The next step to approach the simulation of a real sensor is to use a finished graphene layer also in the transverse direction, passivating the remaining free carbon atoms along the edges of the graphene. I used the same device as previously, so that the results were comparable, with the only difference being the passivation of the edges. (Fig.8.17).

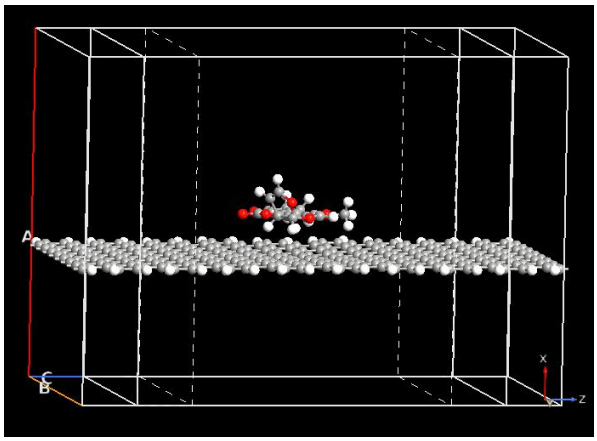

(a) View: perspective

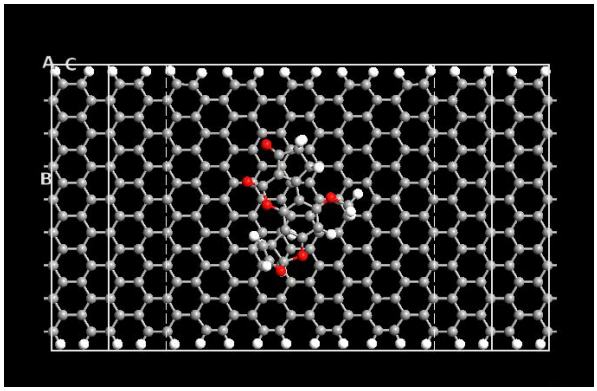

(b) View: from above

Figure 8.17: Passivated graphene device used for simulation with aflatoxin in configuration 1

The orientation of the aflatoxin is that of configuration 1, the most stable after the adsorption process. The white atoms are those of hydrogen. From the trend of the current graph (figure 8.18) it can be seen that the presence of aflatoxin also in this case leads to a reduction of the current in the device up to about 1.3 V where instead there is a change in behavior. For a more precise simulation of a real device, it will be necessary to consider the real dimensions, because the behavior of the graphene nanoribbon changes according to its size. Here I limit myself to considering that around 1.2 V there is a maximum in the current difference which is 2.079 µA. And above 1.3 V the current with aflatoxin increases and at 1.6 V it exceeds that of graphene alone by 5.613 µA.

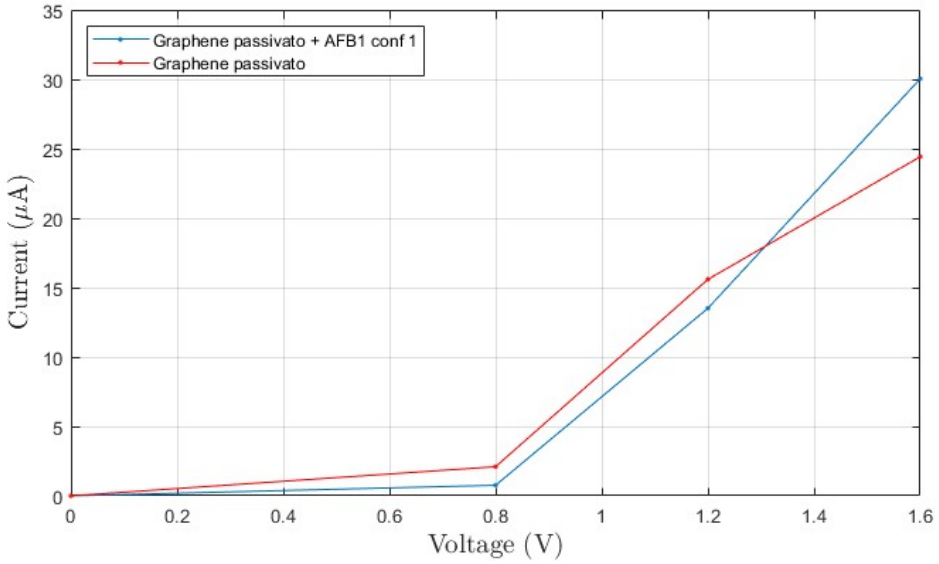

Figure 8.18: Current in passivated graphene and in passivated graphene with aflatoxin in configuration 1

8.1.4 Selectivity

To be such, a sensor must not only guarantee sensitivity with respect to the target molecule, but also selectivity with respect to all the molecules that can be found in the working environment. Selectivity is the property of detecting the target molecule and minimizing the sensitivity with respect to other molecules, at a given bias voltage. To investigate this property in the graphene sensor I analyzed its behavior with respect to some other molecules. A sensor can be used in different environments so it is important to know in which environmental conditions it will have to work because the molecules it will have contact with will be different. It could work for example in solution or in atmosphere. Between these two options, both possible, the first seems the most probable as the first implementation of a sensor for aflatoxin. By making this choice, I investigated the behavior of graphene with respect to some molecules that could be present in a solution: H_2O, Na_2HPO_4, NaCl, KCl.

The first step, as in the study of aflatoxin, was to investigate the adsorption process on a graphene layer for all the molecules. This in order to verify whether the graphene was able to adsorb the molecules and if so, with what force and in which geometric configuration of the adsorbate. So I rotated the molecules in various directions on the graphene, I relaxed the whole system so that it found its equilibrium conformation, I calculated the adsorption energies of the various configurations through formula (7.1) of section 7, to find the most stable configuration between the various molecules and graphene. In the simulations, pseudopotential PseudoDojo with basis set High for Cl and for K was used for better accuracy with respect to these elements according to the indications present in Quantum ATK [48] [49]. In the following, the adsorption energies and the most stable configuration obtained are indicated for each molecule, i.e., with negative adsorption energy but greater in absolute value.

1) H_2O

The adsorption energies per water molecule are presented in the following table (8.1):

Configuration	$\mathbf{E_{ADS}}$ **(kJ/mol)**
A	-11.1318
B	-7.3784
C	-8.0712
D	-12.0156

Table 8.1: Adsorption energies of configuration of H_2O on graphene

The most stable configuration, is the one in which the oxygen atom faces downwards towards the graphene layer. The molecule initially placed at a distance of about 2 Å, after the geometric optimization process, found its equilibrium at a distance of about 3.5 Å from the graphene layer. Figure (8.19) shows the most stable configuration.

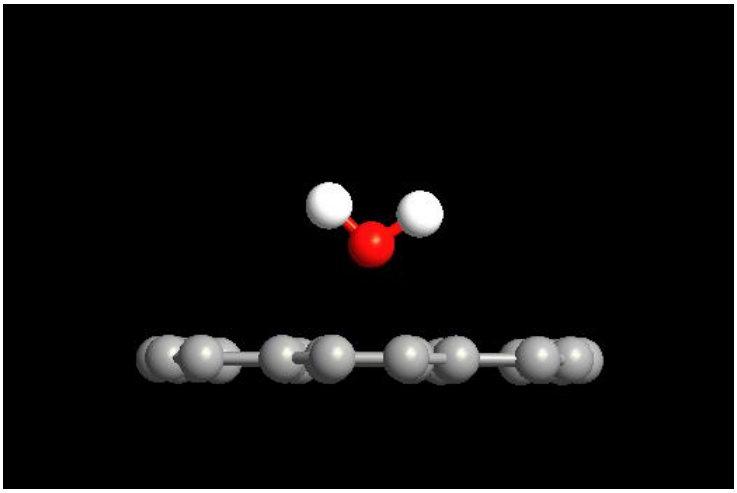

Figure 8.19: Configuration D of H_2O

2) Na_2HPO_4

Na_2HPO_4 is disodium hydrogen phosphate and is a sodium salt of phosphoric acid. Its adsorption energies are presented in the following table (8.2):

Configuration	E_{ADS} (kJ/mol)
A	-83.9463
B	-63.3259
C	-58.8653
D	-79.7964
E	-81.2196

Table 8.2: Adsorption energies of configuration of Na_2HPO_4 on graphene

In the following figure (8.20) its most stable configuration is presented, the one in which the greatest number of atoms are positioned close to the graphene layer. Initially placed at a distance of 2 Å, this molecule also moves away but remaining at a distance of 3 Å.

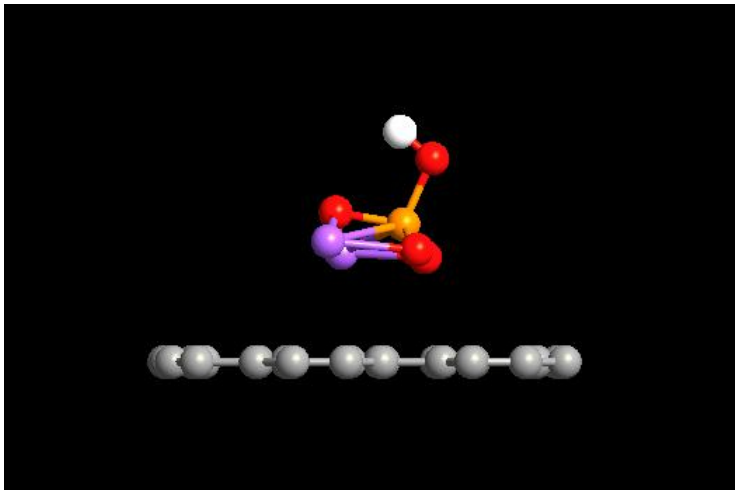

Figure 8.20: Configuration A of Na_2HPO_4

3) NaCl

NaCl is sodium chloride. Its adsorption energies are presented in the following table (8.3):

Configuration	$\mathbf{E_{ADS}}$ **(kJ/mol)**
A	-38.5025
B	-36.9076
C	-28.4417
D	-24.0419

Table 8.3: Adsorption energies of configuration of NaCl on graphene

In the following figure (8.21) its most stable configuration is presented.

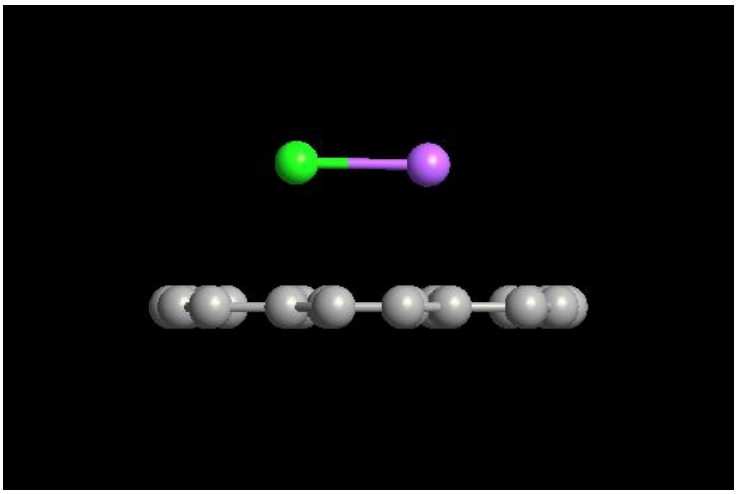

Figure 8.21: Configuration A of NaCl

4) KCl

KCl is potassium chloride. Its adsorption energies are presented in the following table (8.4):

Configuration	E_{ADS} (kJ/mol)
A	-56.2756
B	-42.5280
C	-26.1636
D	-27.7769

Table 8.4: Adsorption energies of configuration of KCl on graphene

In the following figure (8.22) its most stable configuration is presented.

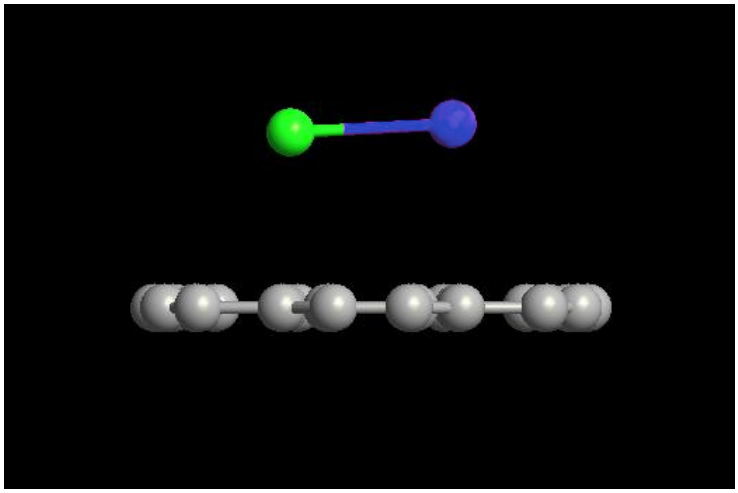

Figure 8.22: Configuration A of KCl

Then I studied the behavior of the current in the presence of these molecules. In the graphs of the currents with molecules other than aflatoxin, only the points are indicated where the simulations reached the convergence with the parameters used for the simulations with aflatoxin. Using the same parameters we have a coherent comparison in the results. I compared them with graphene alone and with graphene plus aflatoxin in configuration 1. The graph in Figure (8.23) shows all the currents obtained in order to be

able to compare the various trends. While in Figure (8.24) shows the square around the voltage of 1.2 V.

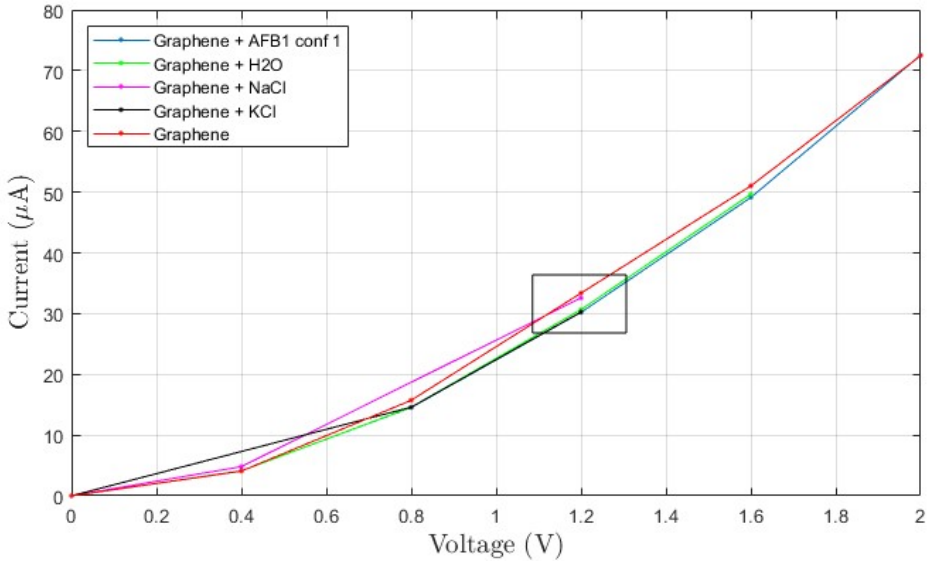

Figure 8.23: Current in Graphene + AFB1 in configuration 1, Graphene + H_2O, Graphene + NaCl, Graphene + KCl, Graphene.

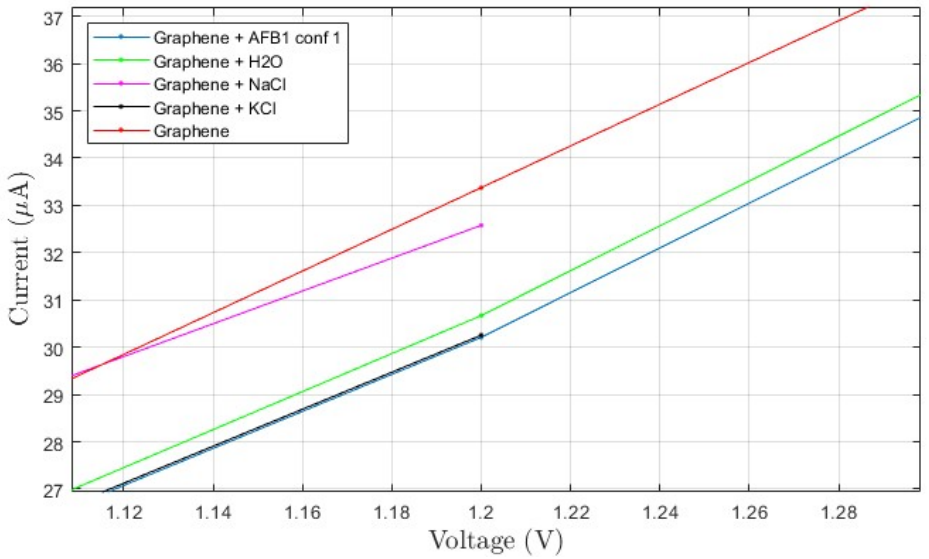

Figure 8.24: Zoom of the current around the voltage of 1.2 V for Graphene + AFB1 in configuration 1, Graphene + H_2O, Graphene + NaCl, Graphene + KCl, Graphene.

From the simulations we can see that the behavior of the water molecule and of potassium chloride is very similar to that of aflatoxin, for all the voltage values taken into consideration and also in correspondence with the voltage of 1.2V. At this bias point, the difference between the current with H_2O and that with aflatoxin is 0.461 µA, while the difference between the current with KCl and that with aflatoxin is even 0.046 µA. The currents are too similar to identify AFB1 with certainty with sufficient reliability. On the other hand, the difference in current between that in the presence of NaCL and that with aflatoxin, which is 2.37 µA to 1.2 V, is quite large. In this case the sensor is selective. Among the molecules considered, the current in the presence of aflatoxin appears to be the one with the lowest current at the voltage considered of 1.2 V.

So even if the selectivity with respect to other molecules such as NaCl is present, graphene as a sensor for the aflatoxin molecule fails in the selectivity with respect to H_2O and a KCl, for the molecules I analyzed. Perhaps the current difference of 0.461 µA with H_2O could still be recognized by a sensor, but not that of only 0.046 µA obtained with KCl. The sensor would not be able to recognize the difference between AFB1 and this molecule.

Chapter 9

Conclusions

Graphene is a material with extraordinary properties that have yet to be fully exploited. Among these is the ability to detect individual molecules.

The research work done in this thesis had the aim of investigating graphene as a possible sensor for the aflatoxin molecule. In the initial part, some theoretical concepts and links to other research related to graphene, aflatoxin, the adsorption process and graphene sensors were provided. Instead, the research work was divided into two parts.

In the first one, the adsorption of the aflatoxin molecule on the graphene was analyzed to verify if they were able to interact with each other and to find the most stable configurations of the system composed of the two.

In the second one, the behavior of graphene as a sensor was investigated. Taking the most stable configurations, the sensitivity was investigated to analyze the current variation in the presence and absence of aflatoxin. It has been verified to have a good sensitivity to the molecule. Then I moved to investigate the selectivity. The behavior of the sensor in the presence of other molecules that could be present in its environment of use was analyzed. It was seen that the trend of the current in the presence of H_2O and mostly KCl molecules was similar to that in the presence of aflatoxin. Based on my simulations, the graphene sensor proves to be sensitive to aflatoxin but it has selectivity problems.

Future work could try to improve the selectivity of graphene. For example, by heating the sensor, molecules with lower adsorption energy than AFB1 should interact with graphene for a short time compared to aflatoxin (this could be the case of H_2O). Instead, in the case of KCl, one could think a buffer with only H_2O and NaCl, therefore without KCl. Also one could think of exploiting the kinetic energy of the molecules through a flow, verifying whether with certain speeds the adsorption of AFB1 is obtained and not that of the other molecules. The general idea to improve the selectivity may be to supply from the outside the energy to the molecules which decreases their adsorption on the graphene compared to that of AFB1. Other future works could investigate functionalized graphene, to try to obtain good sensitivity and at the same time the necessary selectivity.

Bibliography

[1] Chunlei Yan, Qi Wang, and Qingli Yang. Recent advances in aflatoxins detection based on nanomaterials. *Nanomaterials*, 10:1626, 08 2020. doi: 10.3390/nano10091626.

[2] Ning Gan, Jing Zhou, Ping Xiong, Futao Hu, Yuting Cao, Li Tianhua, and Qianli Jiang. An ultrasensitive electrochemiluminescent immunoassay for aflatoxin m1 in milk, based on extraction by magnetic graphene and detection by antibody-labeled cdte quantumn dots-carbon nanotubes nanocomposite. *Toxins*, 5:865–83, 05 2013. doi: 10.3390/toxins5050865.

[3] Xia Xu, Xiangjiang Liu, Yanbin Li, and Yibin Ying. A simple and rapid optical biosensor for detection of aflatoxin b1 based on competitive dispersion of gold nanorods. *Biosensors and Bioelectronics*, 47:361–367, 2013. ISSN 0956-5663. doi: https://doi.org/10.1016/j.bios.2013.03.048. URL https://www.sciencedirect.com/science/article/pii/S0956566313002182.

[4] Xu Wang, Reinhard Niessner, Dianping Tang, and Dietmar Knopp. Review: Nanoparticle-based immunosensors and immunoassays for aflatoxins. *Analytica Chimica Acta*, 912, 02 2016. doi: 10.1016/j.aca.2016.01.048.

[5] Jay Singh, Appan Roychoudhury, Manish Srivastava, Pratima Solanki, Dong-Won Lee, Seung Lee, and Bansi Malhotra. A highly efficient rare earth metal oxide nanorods based platform for aflatoxin detection. *Journal of Materials Chemistry B*, 1:4493, 09 2013. doi: 10.1039/c3tb20690d.

[6] Fabrizio Mo, Chiara Elfi Spano, Yuri Ardesi, Massimo Ruo Roch, Gianluca Piccinini, and Mariagrazia Graziano. Single-molecule aflatoxin b1 sensing via pyrrole-based molecular quantum dot. In *2022 IEEE 22nd International Conference on Nanotechnology (NANO)*, pages 153–156, 2022. doi: 10.1109/NANO54668.2022.9928694.

[7] Ardesi Y Ruo Roch M Piccinini G Graziano M. Mo F, Spano CE. Design of pyrrole-based gate-controlled molecular junctions optimized for single-molecule aflatoxin b1 detection. *Sensors*, 02 2023. doi: 10.3390/s23031687.

[8] Deji Akinwande Hon-Sum Philip Wong. *Carbon Nanotube and Graphene Device Physics*. CAMBRIDGE UNIVERSITY PRESS, 2011.

[9] Lee Jo-won Choi, Wonbong. *Graphene : Synthesis and Applications*. Taylor Francis Group, 2011.

[10] Supriyo Datta. *Quantum Transport*. Cambridge University Press, 2005.

[11] Tsujimura Seiya-Kang Feiyu Inagaki Michio Takai, Kazuyuki. Elsevier, 2020. ISBN 978-0-1281-9576-5. URL https://app.knovel.com/hotlink/toc/id:kpGPPAP004/graphene-preparations/graphene-preparations.

[12] Esrafili Mehdi D. Ehsani Ali Kakaei, Karim. Elsevier, 2019. ISBN 978-0-12-814523-4. URL https://app.knovel.com/hotlink/toc/id:kpGSPC0012/graphene-surfaces-particles/graphene-surfaces-particles.

[13] Changwook Jeong Mark Lundstrom. *Near-Equilibrium Transport*. World Scientific, 2013.

[14] Jie Ma, Dario Alfè, Angelos Michaelides, and Enge Wang. Stone-wales defects in graphene and other planar sp^2-bonded materials. *Phys. Rev. B*, 80:033407, Jul 2009. doi: 10.1103/PhysRevB.80.033407. URL https://link.aps.org/doi/10.1103/PhysRevB.80.033407.

[15] A. M. Valencia and M. J. Caldas. Single vacancy defect in graphene: Insights into its magnetic properties from theoretical modeling. *Phys. Rev. B*, 96:125431, Sep 2017. doi: 10.1103/PhysRevB.96.125431. URL https://link.aps.org/doi/10.1103/PhysRevB.96.125431.

[16] Mark T. Lusk, David T. Wu, and Lincoln D. Carr. Graphene nanoengineering and the inverse stone-thrower-wales defect. *Phys. Rev. B*, 81:155444, Apr 2010. doi: 10.1103/PhysRevB.81.155444. URL https://link.aps.org/doi/10.1103/PhysRevB.81.155444.

[17] Nitrogen doping effects on the structure of graphene. *Applied Surface Science*, 257(21):9193–9198, 2011. ISSN 0169-4332. doi: https://doi.org/10.1016/j.apsusc.2011.05.131. URL https://www.sciencedirect.com/science/article/pii/S0169433211008610.

[18] Hongtao Wang, Qingxiao Wang, Yingchun Cheng, Kun Li, Yingbang Yao, Qiang Zhang, Cezhou Dong, Peng Wang, Udo Schwingenschlögl, Wei Yang, and X. X. Zhang. Doping monolayer graphene with single atom substitutions. *Nano Letters*, 12(1):141–144, 2012. doi: 10.1021/nl2031629. URL https://doi.org/10.1021/nl2031629. PMID: 22136503.

[19] Isabella Gierz, Christian Riedl, U. Starke, Christian Ast, and Klaus Kern. Atomic hole doping of graphene. *Nano letters*, 8:4603–7, 12 2008. doi: 10.1021/nl802996s.

[20] C.A.F. de Oliveira, C.H. Corassin, B. Corrêa, and I.P. Oswald. Animal health: Mycotoxins. In Neal K. Van Alfen, editor, *Encyclopedia of Agriculture and Food Systems*, pages 358–377. Academic Press, Oxford, 2014. ISBN 978-0-08-093139-5. doi: https://doi.org/10.1016/B978-0-444-52512-3.00200-X. URL https://www.sciencedirect.com/science/article/pii/B978044452512300200X.

[21] G. Galaverna and C. Dall'Asta. 4.16 - sampling techniques for the determination of mycotoxins in food matrices. In Janusz Pawliszyn, editor, *Comprehensive Sampling and Sample Preparation*, pages 381–403. Academic Press, Oxford, 2012. ISBN 978-0-12-381374-9. doi: https://doi.org/10.1016/B978-0-12-381373-2.00140-X. URL https://www.sciencedirect.com/science/article/pii/B978012381373200140X.

[22] IARC Working Group on the Evaluation of Carcinogenic Risks to Humans. Some traditional herbal medicines, some mycotoxins, naphthalene and styrene. *IARC monographs on the evaluation of carcinogenic risks to humans*, 82:1–566, 2002.

[23] World Health Organization and Switzerland) Joint FAO/WHO Expert Committee on Food Additives (83rd, 2017: Geneva. *Evaluation of certain contaminants in food: eighty-third report of the Joint FAO/WHO Expert Committee on Food Additives*. World Health Organization, 2017.

[24] M.A. Tirmenstein and R. Mangipudy. Aflatoxin. In Philip Wexler, editor, *Encyclopedia of Toxicology (Third Edition)*, pages 104–106. Academic Press, Oxford, third edition edition, 2014. ISBN 978-0-12-386455-0. doi: https://doi.org/10.1016/B978-0-12-386454-3.00224-4. URL https://www.sciencedirect.com/science/article/pii/B9780123864543002244.

[25] C.D. Williams and H. Jaeschke. Liver toxicology. In J.O. Nriagu, editor, *Encyclopedia of Environmental Health*, pages 509–514. Elsevier, Burlington, 2011. ISBN 978-0-444-52272-6. doi: https://doi.org/10.1016/B978-0-444-52272-6.00294-4. URL https://www.sciencedirect.com/science/article/pii/B9780444522726002944.

[26] M.W. Trucksess and C. Diaz-Amigo. Mycotoxins in foods. In Jerome Nriagu, editor, *Encyclopedia of Environmental Health (Second Edition)*, pages 505–514. Elsevier, Oxford, second edition edition, 2011. ISBN 978-0-444-63952-3. doi: https://doi.org/10.1016/B978-0-444-63951-6.00700-2. URL https://www.sciencedirect.com/science/article/pii/B9780444639516007002.

[27] Paola Battilani, Piero Toscano, HJ (Ine) Van der Fels-Klerx, Antonio Moretti, Marco Camardo Leggieri, Carlo Brera, Agnès Rortais, T.Goumperis, and Tobin Robinson. Aflatoxin b1 contamination in maize in europe increases due to climate change. *Scientific Reports*, 6, 04 2016. doi: 10.1038/srep24328.

[28] Kurt W. Kolasinski. *Surface Science : Foundations of Catalysis and Nanoscience*. John Wiley Sons, Incorporated, 2012.

[29] Ferdinand Huber, Julian Berwanger, Svitlana Polesya, Sergiy Mankovsky, Hubert Ebert, and Franz J. Giessibl. Chemical bond formation showing a transition from physisorption to chemisorption. *Science*, 366:235 – 238, 2019.

[30] Weitkamp Jens Karge, Hellmut G. *Adsorption and Diffusion*. Springer Berlin / Heidelberg, 2008.

[31] L. Yu Kupriyanov. Elsevier, 1996. ISBN 978-0-444-82261-1. URL https://app.knovel.com/hotlink/toc/id:kpSSPCS005/semiconductor-sensors/semiconductor-sensors.

[32] Thomas W. John Crittenden, Barry. *Adsorption Technology and Design*. Elsevier Science Technology, 1998.

[33] Chen Zhongfang Jiang, De-en. *Graphene Chemistry : Theoretical Perspectives*. John Wiley Sons, Incorporated, 2013.

[34] O. Leenaerts, B. Partoens, and F. M. Peeters. Adsorption of h_2O, Nh_3, co, No_2, and no on graphene: A first-principles study. *Phys. Rev. B*, 77:125416, Mar 2008. doi: 10.1103/PhysRevB.77.125416. URL https://link.aps.org/doi/10.1103/PhysRevB.77.125416.

[35] Daniel Dreyer, Sungjin Park, Christopher Bielawski, and Rodney Ruoff. The chemistry of graphene oxide. *Chem. Soc. Rev.*, 39, 12 2009. doi: 10.1039/B917103G.

[36] Niwat Promthong, Chanukorn Tabtimsai, Wandee Rakrai, and Banchob Wanno. Transition metal-doped graphene nanoflakes for co and co2 storage and sensing applications: a dft study. *Structural Chemistry*, 31, 12 2020. doi: 10.1007/s11224-020-01579-9.

[37] S. M. S. Seyyedi, Z. S. Miri Pour, and E. Nadimi. Application of graphene and aluminum doped graphene as a co sensor: An ab initio study. In *2014 22nd Iranian Conference on Electrical Engineering (ICEE)*, pages 463–466, 2014. doi: 10.1109/IranianCEE.2014.6999585.

[38] Tooba Afshari. First-principles studies of ethylene oxide adsorption on pristine and doped graphenes. *Russian Journal of Physical Chemistry*, 12 2022. doi: 10.1134/S0036024422130192DO.

[39] Gui Gui, Jin Li, and Jianxin Zhong. Band structure engineering of graphene by strain: First-principles calculations. *Physical Review B*, 78:075435, 2008.

[40] Ernie W. Hill, Aravind Vijayaragahvan, and Kostya Novoselov. Graphene sensors. *IEEE Sensors Journal*, 11(12):3161–3170, 2011. doi: 10.1109/JSEN.2011.2167608.

[41] Fredrik Schedin, A.K. Geim, S.V. Morozov, Ernie Hill, P Blake, Mikhail Katsnelson, and K.S. Novoselov. Detection of individual gas molecules adsorbed on graphene. *Nature materials*, 6:652–5, 10 2007. doi: 10.1038/nmat1967.

[42] E. H. Hwang, S. Adam, and S. Das Sarma. Transport in chemically doped graphene in the presence of adsorbed molecules. *Phys. Rev. B*, 76:195421, Nov 2007. doi: 10.1103/PhysRevB.76.195421. URL https://link.aps.org/doi/10.1103/PhysRevB.76.195421.

[43] A. Ambrosetti and Pier Silvestrelli. Adsorption of rare-gas atoms and water on graphite and graphene by van der waals-corrected density functional theory. *The Journal of Physical Chemistry C*, 115, 02 2011. doi: 10.1021/jp110669p.

[44] Jiayu Dai and Jianmin Yuan. Physisorption to chemisorption transition of no2 on graphene induced by the interplay of sio2 substrate and van der waals forces: A first principles study. *Chemical Physics*, 405:161–166, 2012. ISSN 0301-0104. doi: https://doi.org/10.1016/j.chemphys.2012.07.008. URL https://www.sciencedirect.com/science/article/pii/S0301010412002765.

[45] Muhammad Haroon Rashid, Ants Koel, and Toomas Rang. Simulations of propane and butane gas sensor based on pristine armchair graphene nanoribbon. *IOP Conference Series: Materials Science and Engineering*, 362:012001, 05 2018. doi: 10.1088/1757-899X/362/1/012001.

[46] T. Wehling, K Novoselov, S Morozov, E. Vdovin, Mikhail Katsnelson, A Geim, and A. Lichtenstein. Molecular doping of graphene. *Nano letters*, 8:173–7, 02 2008. doi: 10.1021/nl072364w.

[47] Søren Smidstrup, Troels Markussen, Pieter Vancraeyveld, Jess Wellendorff, Julian Schneider, Tue Gunst, Brecht Verstichel, Daniele Stradi, Petr A Khomyakov, Ulrik G Vej-Hansen, Maeng-Eun Lee, Samuel T Chill, Filip Rasmussen, Gabriele Penazzi, Fabiano Corsetti, Ari Ojanperä, Kristian Jensen, Mattias L N Palsgaard, Umberto Martinez, Anders Blom, Mads Brandbyge, and Kurt Stokbro. Quantumatk: an integrated platform of electronic and atomic-scale modelling tools. *Journal of Physics: Condensed Matter*, 32(1):015901, oct 2019. doi: 10.1088/1361-648X/ab4007. URL https://dx.doi.org/10.1088/1361-648X/ab4007.

[48] QuantumATK version Q-2019.12, Synopsys QuantumATK (www.synopsys.com/silicon/quantumatk.html).

[49] MJ Van Setten, Matteo Giantomassi, Eric Bousquet, Matthieu J Verstraete, Don R Hamann, Xavier Gonze, and G-M Rignanese. The pseudodojo: Training and grading a 85 element optimized norm-conserving pseudopotential table. *Computer Physics Communications*, 226:39, 2018.